

A Study of Adaptive Modeling Towards Robust Generalization

Zihao Jing¹ Qiuhaao Zeng¹ Ruiyi Fang¹ Yan Yi Li² Yan Sun¹ Boyu Wang¹ Pingzhao Hu^{1,2}

Abstract

Large language models (LLMs) increasingly support reasoning over biomolecular structures, but most existing approaches remain modality-specific and rely on either sequence-style encodings or fixed-length connector tokens for structural inputs. These designs can under-expose explicit geometric cues and impose rigid fusion bottlenecks, leading to over-compression and poor token allocation as structural complexity grows. We present a unified all-atom framework that grounds language reasoning in geometric information while adaptively scaling structural tokens. The method first constructs variable-size structural patches on molecular graphs using an instruction-conditioned gating policy, enabling complexity-aware allocation of query tokens. It then refines the resulting patch tokens via cross-attention with modality embeddings and injects geometry-informed tokens into the language model to improve structure grounding and reduce structural hallucinations. Across diverse all-atom benchmarks, the proposed approach yields consistent gains in heterogeneous structure-grounded reasoning. An anonymized implementation is provided in the supplementary material.

1. Introduction

Background. Multimodal large language models (LLMs) increasingly extend to reason over non-linguistic modalities, including vision, video, and scientific structures. Beyond vision-language models (e.g., Flamingo (Alayrac et al., 2022) and LLaVA (Lin et al., 2024)), recent efforts also target scientific domains, such as Galactica (Taylor et al., 2022) for scientific text, BioGPT (Luo et al., 2022) for biomedical text, and structure-aware models that operate on microscopic geometry, including Mol-Llama (Kim et al., 2025) for molecules, ProtLLM (Zhuo et al., 2024) for proteins,

¹Department of Computer Science, Western University, London, Canada ²Department of Biochemistry, Western University, London, Canada. Correspondence to: Pingzhao Hu <phu49@uwo.ca>.

Preprint. February 6, 2026.

Table 1. Functional group hallucination test on 200 molecules and proteins from dataset GEO-AT. Metrics HR: hallucination rate; HPM: hallucinations per molecule; and AR: answer rate. (S) denotes the model’s sequence-only variant (with tokenizer enhanced). The preferred variant is highlighted in pink for clarity.

MODEL	MOLECULE		MODEL	PROTEIN	
	HR (HPM) ↓	AR ↑		HR (HPM) ↓	AR ↑
MOL-LLAMA(S)	0.28 (0.91)	0.95	PROTCHATGPT(S)	0.34 (0.99)	0.99
MOL-LLAMA	0.12 (0.59)	0.97	PROTCHATGPT	0.10 (0.55)	0.99
3D-MoLM(S)	0.59 (2.23)	0.89	PROT2CHAT(S)	0.29 (2.30)	1.00
3D-MoLM	0.23 (1.15)	0.83	PROT2CHAT	0.06 (0.23)	0.99

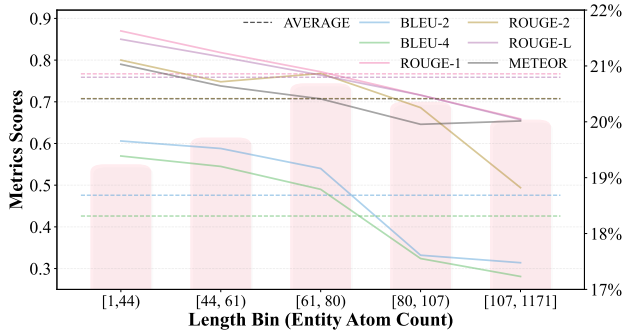


Figure 1. Mol-Llama performance on the Mol-Instructions captioning task, evaluated across five molecule length bins with 6 metrics (left y-axis, detailed in App D.3) plotted as curves with dashed overall averages, and the background bars indicate the proportion of samples in each length bin (right y-axis).

and ChatNT (de Almeida et al., 2025) for nucleic acids.

All-atom modeling has advanced rapidly, catalyzed by AlphaFold-3 (Abramson et al., 2024). Subsequent work, including BoltzGen (Stark et al., 2025) for coordinates generation and ATOMICa (Fang et al., 2025) for representation, further suggests that deep models can operate directly on all-atom level structures. However, most structure-aware LLM efforts remain single modality (Wang et al., 2025b; Park et al., 2024) without a unified interface for heterogeneous all-atom entities. ChatNT (de Almeida et al., 2025) takes a step toward integrating nucleic acids and proteins, but is constrained to sequence inputs without geometric evidence.

This gap motivates a rethinking of how all-atom structural evidence can be selected and exposed to the language model:

Challenge 1: Budget Scaling in All-Atom Modalities.

All-atom graphs span a wide size range. As shown in Fig. 1, Q-Former-style (Li et al., 2023) fixed-length query con-

nectors (Mol-Llama (Kim et al., 2025)) yield lower performance across all metrics for molecules in larger length bins, due to over-compressed geometric features. Conversely, increasing the budget over-allocates capacity to small entities, diluting attention. **Our solution: Scaling-Aware Patching** uses instruction-conditioned gating to select anchors and expand variable-size structural patches, letting the query token budget grow with structural complexity to avoid over-compression and context inefficiency.

Challenge 2: Structural Hallucination. Sequence-only inputs, such as SMILES, protein/DNA residue sequences, do not encode geometry or long-range spatial relations. As shown in Tab. 1, LLMs that lack verifiable structural evidence can produce geometric rationales that are not entailed by the conditioning context. **Our solution: Geometry Grounding Adapter** refines the adaptive tokens through cross-attention with modality embeddings, injecting the final modality tokens into the LLM to provide the explicit geometric grounding to suppress structural hallucinations.

Together, these designs address both the correctness and scalability of structure-aware reasoning: Scaling-Aware Patching adaptively allocates representational capacity to structurally informative regions, while the Geometry Grounding Adapter ensures that LLM outputs are explicitly conditioned on geometry-aware tokens. Our contributions are summarized as follows:

- We propose **Scaling-Aware Patching**, an instruction-conditioned anchor patch growing mechanism ensuring modality token count scales with structural complexity, mitigating fixed-length connector bottlenecks.
- We introduce **Geometry Grounding Adapter**, which injects verifiable geometric cues into the LLM via modality tokens, reducing structural hallucination.
- We present **Cuttlefish**, a unified structure-aware LLM that reasons over all-atom modalities, and achieves strong performance across all-atom understanding benchmarks.

2. Related Work

Molecular LLMs have progressed from contrastive representation learning toward generation and instruction following. MoleculeSTM (Liu et al., 2023b) and MoMu (Su et al., 2022) establish graph or structure and text alignment via contrastive co-embedding, while InstructMol (Cao et al., 2025) and GIT-Mol (Liu et al., 2023a) introduce projector and adapter-based fusion with instruction tuning. Connector designs vary across Q-Former-style (Li et al., 2023) query tokens, as in 3D-MoLM (Li et al., 2024) and Uni-MoT (Guo et al., 2025b), and tokenization oriented bridges such as Graph2Token (Wang et al., 2025a), contrasting with sequence-only baselines like MolT5 (Edwards et al., 2022). Protein LLMs follow a parallel trajectory, from alignment

in ProtST (Xu et al., 2023b) to open-ended generation in ProtLLM (Zhuo et al., 2024), with Prot2Text-V2 (Fei et al., 2025) and ProteinGPT (Xiao et al., 2024a) emphasizing captioning and dialogue under instruction tuning. For nucleic acids, ChatNT (de Almeida et al., 2025) unifies DNA, RNA, and protein through encoder coupling, while RNA-GPT (Xiao et al., 2024b) targets instruction-aligned RNA sequence understanding.

Despite strong empirical progress, existing systems exhibit recurring geometry bottlenecks. Sequence-only or shallow fusion, including MolT5 (Edwards et al., 2022), ProtST (Xu et al., 2023b), and RNA-GPT (Xiao et al., 2024b), often under-specifies geometry, which correlates with structural hallucinations in dialogue settings such as ProtChatGPT (Wang et al., 2024). Embedding-only alignment, as in MoleculeSTM (Liu et al., 2023b), limits expressivity for multi-step reasoning and generation. Simple projection fusion and fixed-length query Q-Former-style (Li et al., 2023) connectors, as in InstructMol (Cao et al., 2025), GIT-Mol (Liu et al., 2023a), 3D-MoLM (Li et al., 2024), Uni-MoT (Guo et al., 2025b), and Chem3DLM (Jiang et al., 2025), compress variable-size structures into a constant token budget, which degrades scalability with entity size and atom-level detail. Discretization-based bridges such as Graph2Token (Wang et al., 2025a) reduce this mismatch but still face information loss at high structural complexity. Several recent variants, including MolCA (Liu et al., 2023c), LLaMo (Park et al., 2024), DeepMolTex (Yan et al., 2025), and Prot2Chat (Wang et al., 2025b), remain within these fixed-capacity connector regimes.

All-atom LLMs must jointly address both structural representation and scaling under variable-length atomistic inputs. This setting demands long-range spatial relations modeling while avoiding information loss from fixed-capacity connectors. Progress likely requires a universal atom-level structural adapter with scaling-aware query length that preserves fine geometry for faithful reasoning. Precise definitions of scaling and modality scope are provided in App. A.3 with detailed related works in App. B.

3. Structure-Grounding All-Atom LLM: Cuttlefish

We introduce Cuttlefish, a structure-aware all-atom LLM. Mirroring the multi-appended versatility of its namesake, Cuttlefish leverages a unified connector that extends to heterogeneous all-atom modalities. Sec. 3.1 introduces the model architecture and the overall data flow, followed by a description of Scaling-Aware Patching in Sec. 3.2 and the Geometry Grounding Adapter in Sec. 3.3. Finally, Sec. 3.4 outlines the training objectives and optimization protocol.

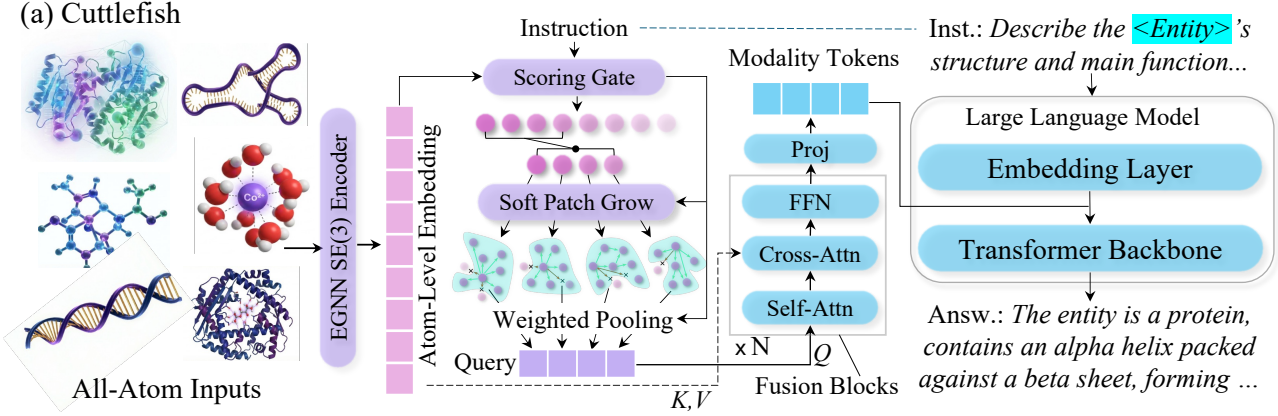


Figure 2. Architecture of Cuttlefish. The framework accepts all-atom inputs (spatial graph: atom features, coordinates, and spatial relations) processed by EGNN for modality embeddings. The model incorporates Scaling-Aware Patching through an instruction-conditioned gate and soft patch-growing mechanism. Then Geometry Grounding Adapter utilizes cross-attention to enrich adaptive tokens with granular geometric features derived from modality embeddings, subsequently projecting these modality tokens into the LLM’s embedding space.

3.1. Architecture Overview

Cuttlefish is a multimodal LLM designed for structure-grounded reasoning by adaptively bridging microscopic geometry with linguistic context. As shown in Fig. 2, (1) input atomic coordinates and features are first encoded via an SE(3)-equivariant Equivariant Graph Neural Network (EGNN) to produce atom-level modality embeddings. (2) Then, an instruction-conditioned scoring gate identifies critical anchor atoms by selecting top-ranking nodes that satisfy a cumulative mass-based threshold. (3) A soft patch-growing operator determines atomic membership using the spatial proximity and gate logits, enabling in-patch weighted pooling to generate structural query tokens. (4) These queries retrieve geometric details through cross-attention to produce modality tokens, which are finally injected into the LLM embedding space at the designated locations.

3.2. Scaling-Aware Patching

The Scaling-Aware Patching compresses all-atom geometry into an adaptive number of tokens by identifying structurally and semantically significant regions. This mechanism addresses the fixed-budget bottleneck by scaling representational capacity relative to the scale of different entities.

Mass-Based Anchor Selection. Given instruction embeddings z , graph-batch assignments b , and SE(3)-equivariant node embeddings \mathbf{X} , we compute per-node anchor logits $\ell = G_{\text{anc}}(z, \mathbf{X}, b)$, which score each atom’s query relevance (Algo. 1, Line 1). For each graph g , we then choose the number of anchors k_g adaptively. Ranking nodes by $\text{prob} = \text{Softmax}(\ell)$, we select the top indices \mathcal{S}_g such that their cumulative probability mass exceeds ρ :

$$k_g = \min \left\{ k \in \{1, \dots, N_g\} \mid \sum_{j=1}^k \text{prob}_{\pi_j} \geq \rho \right\}. \quad (1)$$

where π denotes the descending permutation of prob (Lines 7–8). This cumulative selection ensures further query tokens are adaptively allocated to match the entity scale.

Soft Patch Growth. The identified anchors \mathcal{S}_g are expanded into structural patches via a soft assignment mechanism. We determine the membership $\mathbf{W}_{i,a}$ of atom i to anchor a by fusing spatial proximity with the semantic bias of the anchor (Line 12). The assignment weight is formulated as:

$$\mathbf{W}_{i,a} = \frac{\exp(-\|\mathbf{P}_i - \mathbf{P}_a\|_2^2 + \ell_a)}{\sum_{a' \in \mathcal{S}_g} \exp(-\|\mathbf{P}_i - \mathbf{P}_{a'}\|_2^2 + \ell_{a'})} \quad (2)$$

It ensures that anchors with high instruction relevance (large ℓ_a) can “grow” to capture a wider receptive field, while spatial distances $\|\mathbf{P}_i - \mathbf{P}_a\|_2^2$ (\mathbf{P} is the atom coordinates) maintain geometric locality.

In-Patch Weighted Pooling. Final patch tokens t_a are synthesized through membership-weighted aggregation of node features within each patch:

$$t_a = \sum_{i \in \mathcal{I}_g} \frac{\mathbf{W}_{i,a}}{\sum_{j \in \mathcal{I}_g} \mathbf{W}_{j,a}} \mathbf{X}_i \quad (3)$$

The resulting tokens t_a effectively summarize the structural grounding in both geometry and textual intent, providing a solid query initialization in further retrieval (Sec. 3.3). The gradient rationale of the module is discussed in A.1.

3.3. Geometry Grounding Adapter

The Geometry Grounding Adapter facilitates the explicit injection of geometric evidence into the LLM by transforming

Algorithm 1 Scaling-Aware Patching

Input: Instruction embeddings $\mathbf{z} \in \mathbb{R}^{G \times D_{LLM}}$, node embeddings $\mathbf{X} \in \mathbb{R}^{N \times D_{enc}}$, node coordinates $\mathbf{P} \in \mathbb{R}^{N \times 3}$, batch assignment $\mathbf{b} \in \{0, \dots, G-1\}^N$, anchor gate $g_{anc}(\cdot)$, maximum anchors K_{\max} , mass threshold ρ .

Output: Patch tokens $\mathbf{T} \in \mathbb{R}^{G \times K \times D_{enc}}$, patch mask $\mathbf{M} \in \{0, 1\}^{G \times K}$, anchor indices $\mathbf{A} \in \{1, \dots, N\}^{G \times K}$.

/* Step1: Instruction-Conditioned Anchor Scoring */

- 1: $\ell \leftarrow G_{anc}(\mathbf{z}, \mathbf{X}, \mathbf{b})$ $\triangleright \ell \in \mathbb{R}^N$ anchor logits
- 2: Initialize $\mathbf{T} \leftarrow \mathbf{0}$, $\mathbf{M} \leftarrow \mathbf{0}$, $\mathbf{A} \leftarrow -1$
- /* Step2: Mass-Based Anchor Selection */
- 3: **for** $g = 0$ **to** $G-1$ **do**
- 4: $\mathcal{I}_g \leftarrow \{i \mid b_i = g\}$ \triangleright node indices in graph g
- 5: $\mathbf{p} \leftarrow \text{Softmax}(\ell_{\mathcal{I}_g})$ \triangleright softmax for anchor scoring
- 6: $\pi \leftarrow \text{Argsort}(\mathbf{p}, \text{descending})$ \triangleright sort by score
- 7: $k_g \leftarrow \min(K_{\max}, \min\{k : \sum_{j=1}^k \mathbf{p}_{\pi_j} \geq \rho\})$
- 8: $\mathcal{S}_g \leftarrow \{\mathcal{I}_g[\pi_1], \dots, \mathcal{I}_g[\pi_{k_g}]\}$ \triangleright selected anchors
- /* Step3: Soft Assignment Patch Growth */
- 9: $\mathbf{D}_{i,a} \leftarrow \|\mathbf{P}_i - \mathbf{P}_a\|_2^2 \quad \forall i \in \mathcal{I}_g, a \in \mathcal{S}_g$ \triangleright distance
- 10: $\mathbf{S}_{i,a} \leftarrow -\mathbf{D}_{i,a} + \ell_a \quad \forall i \in \mathcal{I}_g, a \in \mathcal{S}_g$ \triangleright add bias
- 11: $\mathbf{W} \leftarrow \text{Softmax}_a(\mathbf{S})$ \triangleright to assignment weight
- /* Step4: Patch Token Pooling */
- 12: $\mathbf{T}_a \leftarrow \text{Norm}_i(\mathbf{W})^\top \mathbf{X}_{\mathcal{I}_g} \quad \forall a \in \mathcal{S}_g$ \triangleright pooling
- 13: $\mathbf{T}[g, 1:k_g] \leftarrow \{\mathbf{T}_a\}_{a \in \mathcal{S}_g}$, $\mathbf{A}[g, 1:k_g] \leftarrow \mathcal{S}_g$
- 14: $\mathbf{M}[g, 1:k_g] \leftarrow 1$ \triangleright write back pooling results
- 15: **end for**
- 16: **return** $\mathbf{T}, \mathbf{M}, \mathbf{A}$

query tokens from patch pooling into modality tokens.

Geometry Grounding Retrieval. We first project the patch tokens \mathbf{t} from Sec. 3.2 into patch queries \mathcal{Q} (Algo. 2, Line 2). To capture detailed structural dependencies, these queries undergo a series of fusion blocks $\{f_\ell\}_{\ell=1}^{L_f}$ where they execute cross-attention with the full modality embeddings \mathbf{X} (Lines 4–8). This enables queries to retrieve high-resolution geometric cues that are abstracted during patching.

Space Alignment and Injection. The retrieved features are projected into the LLM’s embedding space D_{LLM} as final modality tokens $\widehat{\mathbf{T}}$ (Line 9). We locate the designated injection positions \mathbf{p} corresponding to the modality placeholder y_{ins} within the instruction sequence \mathbf{E} (Line 1). The adapter then inserts the structure-aware tokens $\widehat{\mathbf{T}}$ into the instruction embedding (Lines 10–11). This integration allows Cuttlefish to ground its textual responses in specific structural regions. Analysis from the mutual information aspect is discussed in App. A.2.

3.4. Training

Encoder pretraining (Fig. 3). While the EGNN encoder is not the focus of our novelty, the absence of a unified model

Algorithm 2 Geometry Grounding Adapter

Input: Instruction embeddings $\mathbf{E} \in \mathbb{R}^{B \times L \times D_{LLM}}$, modality (node) embeddings $\mathbf{X} \in \mathbb{R}^{N \times D_{enc}}$, patch tokens \mathbf{T} and patch mask \mathbf{M} (Alg. 1), batch assignment \mathbf{b} , fusion blocks $\{f_\ell\}_{\ell=1}^{L_f}$, modality placeholder token id y_{ins} .

Output: Updated LLM embeddings \mathbf{E}' (and aligned attention/label masks).

/* Step1: Locate Injection Positions */

- 1: $\mathbf{p} \leftarrow \text{FindPos}(\mathbf{y} = y_{ins})$
- /* Step2: Geometry Grounding Retrieval */
- 2: $\mathcal{Q} \leftarrow \text{Proj}_p(\text{Norm}(\mathbf{T}))$ \triangleright get patch queries
- 3: $\mathcal{K}, \mathcal{V} \leftarrow \text{Proj}_n(\text{Norm}(\mathbf{X}))$ \triangleright modality embeddings
- 4: **for** $\ell = 1$ **to** L_f **do**
- 5: $\mathcal{Q} \leftarrow \text{Self-Attn}(\mathcal{Q})$ \triangleright patch tokens themselves
- 6: $\mathcal{Q} \leftarrow \text{Cross-Attn}(\mathcal{Q}, \mathcal{K}, \mathcal{V})$ \triangleright retrieve full nodes
- 7: $\mathcal{Q} \leftarrow \text{FFN}(\mathcal{Q})$
- 8: **end for**
- 9: $\widehat{\mathbf{T}} \leftarrow \text{Norm}_{out}(\text{Proj}_{out}(\mathcal{Q})) \in \mathbb{R}^{G \times K \times D_{LLM}}$
- /* Step3: Inject Geometry Tokens */
- 10: $\mathbf{E}' \leftarrow \text{Insert}(\mathbf{E}, \widehat{\mathbf{T}}, \mathbf{p}; \mathbf{M})$ \triangleright insert K tokens at \mathbf{p}
- 11: Update masks & labels to match \mathbf{E}'
- 12: **return** \mathbf{E}'

capable of processing all-atom modalities necessitated a custom pretraining phase. We adopt an SE(3)-equivariant EGNN as the encoder to ensure the invariance to rotations and translations, which is essential for stable geometric representation. Concretely, for masked atoms and edges, the encoder predicts element identity, pairwise distances, and the injected noise on direction vectors, with total loss:

$$\mathcal{L}_{enc} = \mathcal{L}_{type} + \lambda_d \mathcal{L}_{dist} + \lambda_u \mathcal{L}_{dir}, \quad (4)$$

$$\mathcal{L}_{type} = - \sum_{i \in \mathcal{M}} \log p_\theta(a_i \mid \mathbf{h}_i), \quad (5)$$

$$\mathcal{L}_{dist} = \sum_{(i,j) \in \mathcal{E}_M} \|\hat{d}_{ij} - d_{ij}\|_1, \quad \mathcal{L}_{dir} = \sum_{(i,j) \in \mathcal{E}_M} \|\hat{\epsilon}_{ij} - \epsilon_{ij}\|_2^2, \quad (6)$$

where \mathcal{M} denotes masked atoms, \mathcal{E}_M denotes edges incident to masked atoms, a_i is the element type, $d_{ij} = \|\mathbf{r}_i - \mathbf{r}_j\|_2$ is the interatomic distance, and ϵ_{ij} is the synthetic noise added to a normalized direction vector.

Modality Alignment Tuning (Connector Unfrozen). After encoder pretraining, we freeze the EGNN encoder and the LLM, and optimize only the connector components (Geometry Grounding Adapter and Scaling-Aware Patching) on our all-atom instruction tuning corpus–GEO-AT. This isolates the optimization to the geometry-to-text interface, stabilizes training under all-atom inputs, and allows the connector to learn instruction-conditioned selection and injection without perturbing pretrained linguistic priors.

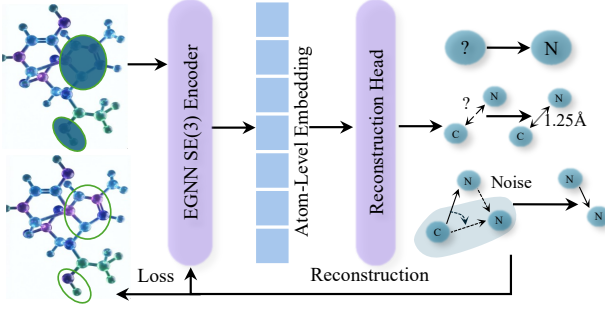


Figure 3. Schematic of all-atom encoder pretraining. Masked reconstruction on all-atom spatial graphs with multi-task heads.

LLM Adaptation Tuning (Connector & LLM Unfrozen). We then unfreeze the LLM and continue end-to-end tuning with a relatively smaller learning rate to let the LLM accommodate the new modality injection distribution while preserving its general language capabilities. Reasoning-related strategy is described in App. C.4.

Unlike Q-Former (Li et al., 2023) style pipelines that require heavy contrastive pretraining to fit a fixed set of learnable query tokens as modality anchors, our structural queries are dynamically instantiated by Scaling-Aware Patching and carry explicit geometric meaning; thus, alignment is achieved directly via instruction supervised end-to-end tuning under variable length query token budgets. Detailed model and training settings are discussed in App. C.1.

4. Experiments

This section evaluates Cuttlefish on heterogeneous all-atom instruction datasets spanning molecules, proteins, and nucleic acids. Training and evaluation data are detailed in Sec. 4.1. Training and optimization performance are analyzed in Sec. 4.2. The performance gains beyond general LLMs are quantified in Sec. 4.3. Comparisons to modality-specific baselines are reported in Sec. 4.4. Scaling ability is discussed in Sec. 4.5, followed by core ablations in Sec. 4.6. Hallucination analysis is in Sec. 4.7 with data contamination analysis in Sec. 4.8.

4.1. Training & Benchmark Datasets

Standard Benchmarks. To fairly compare Cuttlefish with modality-specific baselines, we evaluated on widely adopted benchmarks: (1) **Mol-Instructions** (Fang et al., 2023) aggregates molecules, proteins into a unified instruction format comprising approximately 700K samples verified via human-in-the-loop quality control; (2) **DNA-Chat** (de Almeida et al., 2025) reformulates the Nucleotide Transformer benchmark (Dalla-Torre et al., 2025) into a 7.8M-sample corpus using multi-template question-answering; (3) **RNA-QA** (Xiao et al., 2024b) leverages a topic-modeling summarization pipeline and LLM-based decomposition to generate 400K+ literature-grounded QA pairs from RNA-

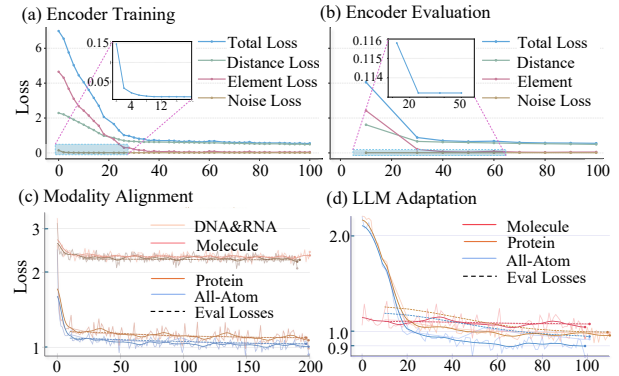


Figure 4. Loss (all atom vs. single modality) across training stages: encoder (a, training; b, evaluation) with objective-wise losses, then modality alignment (c) and LLM adaptation (d). Dashed lines denote evaluation loss. X-axis: global steps (scaled by 0.1).

central (Bateman et al., 2011) for functional annotation. Baselines and selection rationale are discussed in App. D.2.

GEO-AT (ours). Motivated by the absence of corpora with all-atom geometries for LLM tuning, we introduce GEO-AT, the first all-atom instruction dataset encompassing modalities including molecules, proteins, nucleic acids, with atom-level coordinates and language annotations. GEO-AT serves as the training and evaluation data for Cuttlefish, providing a community resource for a geometry-grounded instruction corpus, which will catalyze the next-generation all-atom LLMs. Detailed dataset construction, source, and count are discussed in App. C.2& D.1. Metrics details are in App. D.3.

4.2. Training Performance

Encoder pretraining. Fig. 4 (a,b) shows the encoder training with three objectives with stable and quick convergence, indicating that a huge amount of data is not needed for pretraining to let an encoder learn the spatial relations inside all-atom entities, in line with model MuMo (Jing et al., 2025). For the mask strategy, we also considered masking an appropriate size (multiple residue-level) of graph regions that can capture meaningful long-range relations.

End-to-end tuning. Fig. 4 (c,d) illustrates the loss of two tuning stages. We report the single-modality and mixed-all-atom modality training loss, which shows that the mixed-modality converges better, indicating that *the model can benefit from cross-modality diversity* in complexes and chemical features. Detailed training settings are in App. C.1.

4.3. Cuttlefish vs. General LLMs

To quantify Cuttlefish’s advantage on structural reasoning, representative open-source LLM backbones are compared, including reasoning and non-reasoning variants, on GEO-AT under identical split and finetuning settings, as shown in Tab. 2. Llama-3 (Grattafiori et al., 2024) and Qwen-

Table 2. Improvements compared to general LLM baselines on benchmark GEO-AT across four modalities (molecule, protein, DNA, RNA) measured by METEOR and BERTScore with average scores reported. The best (pink) and second-best (lightpink) are highlighted.

Model	Molecule		Protein		DNA		RNA		Average	
	METEOR	BERT-S	METEOR	BERT-S	METEOR	BERT-S	METEOR	BERT-S	METEOR	BERT-S
<i>General LLM Baselines - Sequence Only - Non-Reasoning</i>										
Qwen-2.5-7B-Instruct	0.137	0.691	0.091	0.651	0.171	0.644	0.159	0.640	0.143	0.653
Llama-3.1-8B-Instruct	0.229	0.778	0.178	0.742	0.175	0.658	0.175	0.646	0.186	0.694
Mistral-3-8B-Instruct-2512	0.185	0.732	0.134	0.714	0.156	0.665	0.192	0.652	0.172	0.683
GLM-4-9B-0414	0.174	0.644	0.110	0.672	0.204	0.690	0.143	0.549	0.155	0.621
<i>General LLM Baselines - Reasoning - Sequence Only</i>										
Qwen3-8B	0.103	0.715	0.044	0.679	0.131	0.665	0.128	0.655	0.107	0.674
DeepSeek-R1-D-Qwen-7B	0.160	0.721	0.141	0.707	0.206	0.659	0.170	0.687	0.169	0.692
Mistral-3-8B-Reasoning-2512	0.147	0.753	0.108	0.811	0.264	0.806	0.180	0.674	0.176	0.744
<i>General LLM Baselines - Reasoning - Sequence Only - Modality Enhanced Tokenizer</i>										
Qwen3-8B	0.158	0.709	0.027	0.573	0.177	0.792	0.095	0.773	0.110	0.724
DeepSeek-R1-D-Qwen-7B	0.204	0.673	0.219	0.617	0.147	0.644	0.283	0.688	0.227	0.662
Mistral-3-8B-Reasoning-2512	0.185	0.823	0.192	0.755	0.149	0.756	0.288	0.579	0.220	0.698
<i>Ours</i>										
Cuttlefish + Qwen2.5-7B	0.314	0.863	0.317	0.816	0.262	0.806	0.378	0.858	0.330	0.840
Cuttlefish + Llama-3.1-8B-I	0.391	0.875	0.417	0.896	0.529	0.816	0.403	0.868	0.428	0.864
Cuttlefish + Mistral-3-8B-I	0.415	0.653	0.333	0.858	0.358	0.852	0.220	0.694	0.310	0.750
Cuttlefish + GLM-4-9B	0.327	0.830	0.262	0.831	0.443	0.888	0.403	0.794	0.367	0.827
Cuttlefish + Qwen3-8B	0.389	0.853	0.377	0.888	0.391	0.860	0.491	0.890	0.428	0.876
Cuttlefish + R1-7B	0.342	0.812	0.327	0.801	0.330	0.802	0.422	0.799	0.369	0.803
Cuttlefish + Mistral3-8B-R	0.309	0.776	0.320	0.756	0.256	0.798	0.395	0.775	0.335	0.776

3 (Yang et al., 2025a) exhibit relatively strong bio-modality understanding, motivating the adoption of Llama-3.1 as the default backbone in subsequent experiments. To mitigate sequence-level comprehension difficulty for general LLMs, a modality tokenizer is introduced that maps meaningful motifs or residues to single tokens, yielding consistent performance gains. Across different backbones, augmenting with Cuttlefish produces substantial improvements on each modality and the average, supporting **two conclusions**: (1) atom-level modalities require structure-enhanced understanding beyond sequence representation, and (2) Cuttlefish enables stronger multimodal reasoning over heterogeneous all-atom modalities. *Supports Tackling Challenge 2: Structural Grounding*.

4.4. Cuttlefish vs. Modality-Specific Baselines

Cuttlefish is evaluated on all 17 Mol-Instruction (Fang et al., 2023) tasks, 20 tasks from DNA-Chat (de Almeida et al., 2025) and RNA-QA (Xiao et al., 2024b), comparing against modality-specific models.

Small molecules (Tab. 3). Performance is reported against benchmark baselines and strong molecular LLMs such as Mol-Llama (Kim et al., 2025). Covered tasks span molecular captioning, description-guided design, reaction-related prediction, QA, true-or-false, and multiple-choice settings, reflecting broad molecular understanding and instruction following performance. Full metrics results see App. D.4.

Proteins (Tab. 4). Evaluation uses five protein tasks from Mol-Instruction (Fang et al., 2023). Provided inputs are pro-

tein sequences; structures are retrieved by mapping UniProt IDs (Consortium, 2019) to PDB IDs (Burley et al., 2017). For targets missing PDB structures, AlphaFold2 (Jumper et al., 2021) is used to generate structures. Cuttlefish enables superior reasoning over both sequence-only and Q-Former style multimodal LLM baselines.

Nucleic acids. DNA evaluation follows the DNA-Chat (de Almeida et al., 2025) dataset, covering 18 tasks. As shown in Fig. 5 (a) Cuttlefish achieves top-1 average performance, slightly exceeding ChatNT (de Almeida et al., 2025). Limited gains from atom-level inputs are consistent with substantial structural repetition in DNA. Per-task results are summarized in Fig. 5 (b). For RNA (Tab. 5), Cuttlefish is validated on benchmark RNA-QA (Xiao et al., 2024b).

Across modalities, Cuttlefish attains top-1 results on most tasks, indicating unified all-atom understanding surpasses modality-specific single domain models, and validating the structural grounding design for all-atom reasoning. *Supports Tackling Challenge 2: Structural Grounding*.

4.5. Scaling Stability and Token Efficiency

Scaling Stability. Figs 6 (a–b) illustrate modality scaling results on two Mol-Instructions (Fang et al., 2023) generation tasks (molecular captioning and protein functional description), where test instances are stratified into graph node-count bins to evaluate performance under increasing structural complexity. Across these varied bins, Cuttlefish maintains remarkably stable generation quality and achieves its most significant relative gains in the high-size regime,

Table 3. Performance on the Mol-Instructions molecule-related benchmark. Design, Forward, Retro, and Reagent denote molecular design, forward prediction, retrosynthesis, and reagent prediction, each reported by validity (Val) and RDKit fingerprint similarity (FTS). OpenQA reports BERTScore. T/F and MC denote True-or-False and Multi-Choice accuracy, and ER and IE denote Entity Recognition and Interaction Extraction F1. The best (pink) and second-best (lightpink) results are highlighted. Full metrics results see App. D.4

Model	Captioning		Design		Forward		Retro		Reagent		OpenQA	T/F	MC	ER	IE
	ROUGE-L↑	METEOR↑	Val↑	FTS↑	Val↑	FTS↑	Val↑	FTS↑	Val↑	FTS↑					
Alpaca-7B	0.136	0.107	0.002	0.006	0.138	0.004	0.160	0.005	0.186	0.029	0.824	0.330	0.290	0.210	0.040
Baize-7B	0.148	0.106	0.002	0.000	0.097	0.004	0.112	0.025	0.099	0.022	0.811	0.480	0.240	0.010	0.000
ChatGLM-6B	0.166	0.129	0.005	0.005	0.108	0.050	0.046	0.056	0.074	0.017	0.795	0.180	0.220	0.150	0.020
Llama-3-8B	0.148	0.184	0.003	0.005	0.039	0.001	0.010	0.018	0.001	0.037	0.814	0.270	0.300	0.000	0.050
Vicuna-v1.5-13B	0.130	0.168	0.001	0.006	0.059	0.007	0.017	0.025	0.007	0.038	0.814	0.120	0.290	0.020	0.080
Galactica-6.7B	0.063	0.065	0.992	0.135	0.946	0.156	0.984	0.167	0.995	0.036	0.794	0.420	0.310	0.170	0.030
Qwen-2.5-7B	0.572	0.538	0.772	0.207	0.953	0.163	0.939	0.168	0.997	0.258	0.846	0.210	0.870	0.400	0.170
MolIT5	0.034	0.033	0.773	0.400	-	-	-	-	-	-	0.615	0.350	0.490	0.540	0.120
Mol-Ins.-Llama-2	0.291	0.291	1.000	0.231	1.000	0.313	1.000	0.283	1.000	0.237	0.837	0.550	0.650	0.750	0.220
Mol-Ins.-Llama-3.1	0.709	0.637	1.000	0.358	1.000	0.756	1.000	0.704	1.000	0.412	0.846	0.600	0.960	0.690	0.180
Mol-LLama-2	0.750	0.701	0.876	0.254	1.000	0.724	1.000	0.362	1.000	0.256	0.823	0.560	0.850	0.740	0.210
Mol-LLama-3.1	0.759	0.707	0.953	0.392	1.000	0.774	1.000	0.708	1.000	0.411	0.812	0.600	0.880	0.700	0.200
Cuttlefish	0.766	0.715	1.000	0.422	1.000	0.792	1.000	0.747	1.000	0.509	0.884	0.660	0.890	0.780	0.270

Table 4. Protein-oriented Mol-Instructions benchmarks. IE denotes interaction extraction. PF, FD, CA, and DM denote protein function, functional description, catalytic activity, and domain or motif prediction. The top-2 are highlighted in pink and lightpink.

Model	IE	PF	FD	CA	DM
	F1↑	ROUGE-L↑	ROUGE-L↑	ROUGE-L↑	ROUGE-L↑
Alpaca-7B	0.002	0.200	0.100	0.230	0.120
Baize-7B	0.004	0.200	0.150	0.220	0.130
ChatGLM-6B	0.003	0.150	0.140	0.130	0.100
Llama-3-8B	0.003	0.120	0.120	0.130	0.090
Vicuna-v1.5-13B	0.013	0.150	0.140	0.160	0.120
Galactica-6.7B	0.001	0.070	0.080	0.080	0.060
Mol-Instructions	0.224	0.430	0.440	0.520	0.460
ProtLLM	0.176	0.450	0.435	0.463	0.384
ProteinGPT	0.166	0.336	0.416	0.406	0.472
ProtChatGPT	0.055	0.355	0.510	0.306	0.452
Cuttlefish	0.273	0.486	0.520	0.551	0.495

signaling favorable scaling characteristics rather than the size-induced degradation often seen in fixed-capacity models. This trend is directly attributable to Scaling-Aware Patching: by implementing a variable query token budget rather than enforcing a rigid fixed-length bottleneck, the connector adaptively preserves critical fine-grind features regardless of the entity’s scale.

Token Efficiency. Fig. 6 (c) reports the language/structure token fractions and Fig. 6 (d) shows the modality token usage as entity size increases. Compared to a strong baseline ChatNT (de Almeida et al., 2025), which scales token count linearly, Cuttlefish maintains a substantially lower structural token budget while scaling reasonably with the entity size. Detailed training, token and memory efficiency analysis see App. D.7. *Supports Tackling Challenge 1: Budget Scaling.*

4.6. Main Ablations

Settings. Tab. 6 reports the core ablations of Cuttlefish, including: (i) single-modality instead of mixed all-atom, (ii) residue-level chemically meaningful patches in place of the proposed patching, (iii) removal of instruction guidance

Table 5. Performance on two data types from RNA-QA: Abstract Information Summary (AIS) and Divide and Conquer RNA Literature Summarization (D&C), evaluated by ROUGE-1/2/L. The best (pink) and second-best (lightpink) results are highlighted.

Baseline	RNA-QA (AIS)			RNA-QA (D&C)		
	ROUGE-1↑	ROUGE-2↑	ROUGE-L↑	ROUGE-1↑	ROUGE-2↑	ROUGE-L↑
Llama3-8B	0.236	0.094	0.204	0.247	0.096	0.218
RNA-FM	0.224	0.136	0.209	0.092	0.039	0.080
RNA-GPT	0.503	0.367	0.475	0.479	0.269	0.441
Cuttlefish	0.494	0.371	0.512	0.519	0.432	0.471

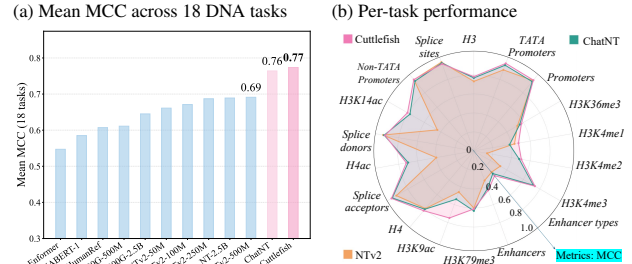


Figure 5. Evaluation on DNA-Chat. (a) Mean Matthews correlation coefficient (MCC) over 18 DNA tasks, comparing Cuttlefish with representative baselines (x-axis). (b) Per-task MCC on the same 18 tasks, overlaying Cuttlefish and top-2 baselines.

in the anchor gate, (iv) removal of the fusion blocks, (v) replacement of the connector with standard Q-Former (Li et al., 2023), (vi) a sequence-only baseline with the enhanced tokenizer, and (vii) removal of soft patch growth.

Results. Single-modality training yields the smallest degradation, indicating that the architecture remains effective under unimodal inputs, while mixed-modality training provides additional gains, consistent with cross-entity transfer of chemical relations. Residue-level patching incurs a 10% drop, suggesting that chemically meaningful segmentation is not optimal under the target objectives and that lack of instruction conditioning limits focus allocation.

Combined ablations further substantiate the necessity of

Table 6. Ablation study on generation quality across modalities, evaluated by METEOR and BERTScore. DNA&RNA aggregates nucleic acids. Avg. Drop reports relative degradation from the full model. The best (pink) and second-best (lightpink) results are highlighted.

Ablation	Molecule		Protein		DNA&RNA		Average		Avg. Drop (%)	
	METEOR↑	BERTScore↑	METEOR↑	BERTScore↑	METEOR↑	BERTScore↑	METEOR↑	BERTScore↑	METEOR	BERTScore
Cuttlefish	0.391	0.875	0.417	0.896	0.466	0.842	0.425	0.871	-	-
Single-modality encoder	0.387	0.845	0.424	0.876	0.435	0.821	0.415	0.847	2.17	2.69
Residue-level patching	0.320	0.746	0.368	0.820	0.452	0.771	0.380	0.779	10.49	10.53
w/o instruction-guided gating	0.309	0.791	0.338	0.814	0.448	0.748	0.365	0.785	14.01	9.89
w/o fusion blocks	0.310	0.796	0.342	0.815	0.355	0.678	0.336	0.763	20.96	12.38
Q-Former variant (same max token length)	0.332	0.856	0.218	0.774	0.174	0.687	0.241	0.772	43.15	11.31
Sequence-only baseline	0.229	0.778	0.178	0.742	0.175	0.652	0.194	0.724	54.32	16.83
Seq-only + enhanced tokenizer	0.203	0.699	0.141	0.494	0.218	0.731	0.187	0.701	55.89	19.46
w/o soft patch growth	0.136	0.675	0.123	0.686	0.163	0.662	0.141	0.674	66.83	22.57

Table 7. Functional group hallucination test on 200 molecules and proteins from dataset GEO-AT. Metrics HR: hallucination rate; HPM: hallucinations per molecule; and AR: answer rate.

MOLECULE			PROTEIN				
MODEL	HR ↓	HPM ↓	AR ↑	MODEL	HR ↓	HPM ↓	AR ↑
MOL-LLAMA	0.12	0.59	0.94	PROTCHATGPT	0.10	0.55	0.94
3D-MOLM	0.23	1.15	0.83	PROT2CHAT	0.06	0.23	0.95
CUTTLEFISH	0.07	0.17	0.99	CUTTLEFISH	0.04	0.17	0.97

both proposed novelties. The Q-Former connector performs competitively on molecules but degrades on proteins and nucleic acids, consistent with a fixed-length bottleneck as structural complexity increases. Finally, the sequence-only baseline underperforms, supporting the claim that sequence-only inputs are insufficient. Extended ablation experiments are discussed in App. E.

4.7. Hallucination Analysis

We evaluate hallucination on 200 molecules and proteins sampled from GEO-AT (Tab. 7) against strong domain-specific baselines. Across both modalities, Cuttlefish achieves the lowest hallucination rate, while maintaining the highest answer rate, indicating improved robustness to structural hallucination under comparable task settings. Detailed reasoning examples are discussed in App. D.5. *Supports Tackling Challenge 2: Structural Grounding.*

4.8. Data Contamination Analysis

Data contamination is a common problem in large language model training. To prevent data contamination, we think that in our encoder training and alignment tuning, the performance is not that data-dependent, as we are not telling the models to learn new knowledge, but rather the ability to recognize chemical structures and match them to language knowledge (details in App. D.6). And to ensure a fair comparison, we remove all the benchmark test set data indexed by entity in our training set, and use a 13-gram overlap test (Brown et al., 2020) to process as well. To prove the effectiveness of letting LLM understand structures, we use the same corpus to train LLM without Cuttlefish structural components to prove that the performance improvements are not affected by LLM’s pretrained knowledge itself (Tab. 2).

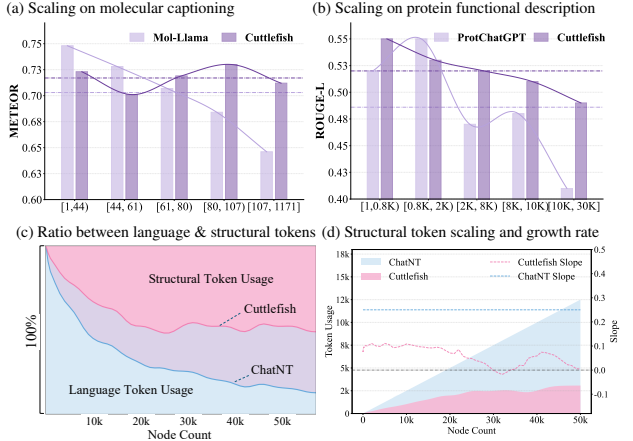


Figure 6. Scaling analysis by entity size. (a-b) Mol-Instructions results for Cuttlefish versus task-specific strong baselines on molecular & protein captioning tasks, plotted over atom-count bins (x-axis); bars show bin-wise scores (METEOR / ROUGE-L), with dashed lines indicating averages and solid curves indicating trend lines. (c-d) Scaling versus ChatNT over the node-count axis: (c) language/structural token fractions, and (d) structural-token usage (area) with growth-rate indicators (dashed).

5. Conclusion

Cuttlefish establishes a unified framework for structure-grounded reasoning across all-atom modalities. By integrating Scaling-Aware Patching, the architecture enables instruction-conditioned query token scaling, bypassing fixed-length connector bottlenecks while preserving fine-grained structural signals. Building on these adaptive representations, Geometry Grounding Adapter injects verifiable geometric cues into the LLM to mitigate structural hallucinations. Empirical results across all-atom modality benchmarks show consistent gains, and support four observations: (1) sequence-only inputs are insufficient and (2) fixed-length connectors impose an information bottleneck for capturing geometry-dependent semantics; (3) Structural-aware LLMs can internalize atom-level structural features with appropriate alignment, and (4) joint modality training improves per-modality learning. Overall, these findings indicate that Scaling-Aware Patching and Geometry Grounding Adapter are key to robust, unified multimodal scientific reasoning. Limitations and future works are discussed in App. F.

Impact Statement

This paper aims to advance machine learning by improving structure-aware LLMs for all-atom modalities. It introduces mechanisms that ground language reasoning in geometric evidence and scale modality tokens with structural complexity to improve faithfulness and scalability. The work is intended for general scientific modeling settings, and no broader societal impacts beyond those common to this research area are expected.

References

Abramson, J., Adler, J., Dunger, J., Evans, R., Green, T., Pritzel, A., Ronneberger, O., Willmore, L., Ballard, A. J., Bambrick, J., et al. Accurate structure prediction of biomolecular interactions with alphafold 3. *Nature*, 630 (8016):493–500, 2024.

Alayrac, J.-B., Donahue, J., Luc, P., Miech, A., Barr, I., Hasson, Y., Lenc, K., Mensch, A., Millican, K., Reynolds, M., et al. Flamingo: a visual language model for few-shot learning. *Advances in neural information processing systems*, 35:23716–23736, 2022.

Bai, S., Chen, K., Liu, X., Wang, J., Ge, W., Song, S., Dang, K., Wang, P., Wang, S., Tang, J., et al. Qwen2. 5-vl technical report. *arXiv preprint arXiv:2502.13923*, 2025.

Bateman, A., Agrawal, S., Birney, E., Bruford, E. A., Bujnicki, J. M., Cochrane, G., Cole, J. R., Dinger, M. E., Enright, A. J., Gardner, P. P., et al. Rnacentral: a vision for an international database of rna sequences. *Rna*, 17 (11):1941–1946, 2011.

Brown, T., Mann, B., Ryder, N., Subbiah, M., Kaplan, J. D., Dhariwal, P., Neelakantan, A., Shyam, P., Sastry, G., Askell, A., et al. Language models are few-shot learners. *Advances in neural information processing systems*, 33: 1877–1901, 2020.

Burley, S. K., Berman, H. M., Kleywegt, G. J., Markley, J. L., Nakamura, H., and Velankar, S. Protein data bank (pdb): the single global macromolecular structure archive. *Protein crystallography: methods and protocols*, pp. 627–641, 2017.

Cao, H., Liu, Z., Lu, X., Yao, Y., and Li, Y. Instructml: Multi-modal integration for building a versatile and reliable molecular assistant in drug discovery. In *Proceedings of the 31st International Conference on Computational Linguistics*, pp. 354–379, 2025.

Christofidellis, D., Giannone, G., Born, J., Winther, O., Laino, T., and Manica, M. Unifying molecular and textual representations via multi-task language modelling. In *International Conference on Machine Learning*, pp. 6140–6157. PMLR, 2023.

Consortium, U. Uniprot: a worldwide hub of protein knowledge. *Nucleic acids research*, 47(D1):D506–D515, 2019.

Dalla-Torre, H., Gonzalez, L., Mendoza-Revilla, J., Lopez Carranza, N., Grzywaczewski, A. H., Oteri, F., Dallago, C., Trop, E., de Almeida, B. P., Sirelkhatim, H., et al. Nucleotide transformer: building and evaluating robust foundation models for human genomics. *Nature Methods*, 22(2):287–297, 2025.

de Almeida, B. P., Richard, G., Dalla-Torre, H., Blum, C., Hexemer, L., Pandey, P., Laurent, S., Rajesh, C., Lopez, M., Laterre, A., et al. A multimodal conversational agent for dna, rna and protein tasks. *Nature Machine Intelligence*, pp. 1–14, 2025.

Edwards, C., Lai, T., Ros, K., Honke, G., Cho, K., and Ji, H. Translation between molecules and natural language. *arXiv preprint arXiv:2204.11817*, 2022.

Fang, A., Zhang, Z., Zhou, A., and Zitnik, M. Atomica: Learning universal representations of intermolecular interactions. *bioRxiv*, pp. 2025–04, 2025.

Fang, Y., Liang, X., Zhang, N., Liu, K., Huang, R., Chen, Z., Fan, X., and Chen, H. Mol-instructions: A large-scale biomolecular instruction dataset for large language models. *arXiv preprint arXiv:2306.08018*, 2023.

Fei, X., Chatzianastasis, M., Carneiro, S. A., Abdine, H., Petalidis, L. P., and Vazirgiannis, M. Prot2text-v2: Protein function prediction with multimodal contrastive alignment. *arXiv preprint arXiv:2505.11194*, 2025.

Gao, B., Huang, Y., Liu, Y., Xie, W., He, B., Tan, H., Ma, W.-Y., Zhang, Y.-Q., and Lan, Y. Cidd: Collaborative intelligence for structure-based drug design empowered by llms. In *The Thirty-ninth Annual Conference on Neural Information Processing Systems*, 2025.

GLM, T., Zeng, A., Xu, B., Wang, B., Zhang, C., Yin, D., Zhang, D., Rojas, D., Feng, G., Zhao, H., et al. Chatglm: A family of large language models from glm-130b to glm-4 all tools. *arXiv preprint arXiv:2406.12793*, 2024.

Grattafiori, A., Dubey, A., Jauhri, A., Pandey, A., Kadian, A., Al-Dahle, A., Letman, A., Mathur, A., Schelten, A., Vaughan, A., et al. The llama 3 herd of models. *arXiv preprint arXiv:2407.21783*, 2024.

Guo, D., Yang, D., Zhang, H., Song, J., Zhang, R., Xu, R., Zhu, Q., Ma, S., Wang, P., Bi, X., et al. Deepseek-r1: Incentivizing reasoning capability in llms via reinforcement learning. *arXiv preprint arXiv:2501.12948*, 2025a.

Guo, H., Huo, M., Zhang, R., and Xie, P. Proteinchat: Towards achieving chatgpt-like functionalities on protein 3d structures. *Authorea Preprints*, 2023.

Guo, S., Bian, Y., Wang, R., Yin, N., Wang, Z., and Yao, Q. Unified molecule-text language model with discrete token representation. In *Proceedings of the Thirty-Fourth International Joint Conference on Artificial Intelligence*, pp. 9205–9213, 2025b.

Inoue, Y., Song, T., Wang, X., Luna, A., and Fu, T. Drugagent: Multi-agent large language model-based reasoning for drug-target interaction prediction. *ArXiv*, pp. arXiv-2408, 2025.

Jiang, L., Sun, S., Qi, B., Fu, Y., Xu, X., Li, Y., Zhou, D., and Fu, T. Chem3dilm: 3d multimodal large language models for chemistry. *arXiv preprint arXiv:2508.10696*, 2025.

Jing, Z., Sun, Y., Li, Y. Y., Janarthanan, S., Deng, A., and Hu, P. Structure-aware fusion with progressive injection for multimodal molecular representation learning. *arXiv preprint arXiv:2510.23640*, 2025.

Joshi, C. K., Fu, X., Liao, Y.-L., Gharakhanyan, V., Miller, B. K., Sriram, A., and Ulissi, Z. W. All-atom diffusion transformers: Unified generative modelling of molecules and materials. *arXiv preprint arXiv:2503.03965*, 2025.

Jumper, J., Evans, R., Pritzel, A., Green, T., Figurnov, M., Ronneberger, O., Tunyasuvunakool, K., Bates, R., Žídek, A., Potapenko, A., et al. Highly accurate protein structure prediction with alphafold. *nature*, 596(7873):583–589, 2021.

Kim, D., Lee, W., and Hwang, S. J. Mol-llama: Towards general understanding of molecules in large molecular language model. *arXiv preprint arXiv:2502.13449*, 2025.

Kim, S., Chen, J., Cheng, T., Gindulyte, A., He, J., He, S., Li, Q., Shoemaker, B. A., Thiessen, P. A., Yu, B., et al. Pubchem 2023 update. *Nucleic acids research*, 51(D1): D1373–D1380, 2023.

Landrum, G. Rdkit documentation. *Release*, 1(1-79):4, 2013.

Li, J., Li, D., Savarese, S., and Hoi, S. Blip-2: Bootstrapping language-image pre-training with frozen image encoders and large language models. In *International conference on machine learning*, pp. 19730–19742. PMLR, 2023.

Li, S., Liu, Z., Luo, Y., Wang, X., He, X., Kawaguchi, K., Chua, T.-S., and Tian, Q. Towards 3d molecule-text interpretation in language models. *arXiv preprint arXiv:2401.13923*, 2024.

Lin, B., Ye, Y., Zhu, B., Cui, J., Ning, M., Jin, P., and Yuan, L. Video-llava: Learning united visual representation by alignment before projection. In *Proceedings of the 2024 conference on empirical methods in natural language processing*, pp. 5971–5984, 2024.

Liu, A. H., Khandelwal, K., Subramanian, S., Jouault, V., Rastogi, A., Sadé, A., Jeffares, A., Jiang, A., Cahill, A., Gavaudan, A., et al. Minstral 3. *arXiv preprint arXiv:2601.08584*, 2026.

Liu, P., Ren, Y., and Ren, Z. Git-mol: A multi-modal large language model for molecular science with graph. *Image, and Text*, 2023a.

Liu, S., Nie, W., Wang, C., Lu, J., Qiao, Z., Liu, L., Tang, J., Xiao, C., and Anandkumar, A. Multi-modal molecule structure–text model for text-based retrieval and editing. *Nature Machine Intelligence*, 5(12):1447–1457, 2023b.

Liu, Z., Li, S., Luo, Y., Fei, H., Cao, Y., Kawaguchi, K., Wang, X., and Chua, T.-S. Molca: Molecular graph-language modeling with cross-modal projector and unimodal adapter. *arXiv preprint arXiv:2310.12798*, 2023c.

Luo, R., Sun, L., Xia, Y., Qin, T., Zhang, S., Poon, H., and Liu, T.-Y. Biogpt: generative pre-trained transformer for biomedical text generation and mining. *Briefings in bioinformatics*, 23(6):bbac409, 2022.

Park, J., Bae, M., Ko, D., and Kim, H. J. Llamo: Large language model-based molecular graph assistant. *Advances in Neural Information Processing Systems*, 37: 131972–132000, 2024.

Pei, Q., Yan, R., Gao, K., Zhu, J., and Wu, L. 3d-molt5: Leveraging discrete structural information for molecule-text modeling. *arXiv preprint arXiv:2406.05797*, 2024.

Senior, A. W., Evans, R., Jumper, J., Kirkpatrick, J., Sifre, L., Green, T., Qin, C., Žídek, A., Nelson, A. W., Bridgland, A., et al. Improved protein structure prediction using potentials from deep learning. *Nature*, 577(7792): 706–710, 2020.

Stark, H., Faltings, F., Choi, M., Xie, Y., Hur, E., O’Donnell, T., Bushuiev, A., Uçar, T., Passaro, S., Mao, W., et al. Boltzgen: Toward universal binder design. *bioRxiv*, pp. 2025–11, 2025.

Su, B., Du, D., Yang, Z., Zhou, Y., Li, J., Rao, A., Sun, H., Lu, Z., and Wen, J.-R. A molecular multimodal foundation model associating molecule graphs with natural language. *arXiv preprint arXiv:2209.05481*, 2022.

Tang, Y., Xu, W., Cao, J., Gao, W., Farrell, S., Erichson, B., Mahoney, M. W., Nonaka, A., and Yao, Z. Matterchat: A multi-modal llm for material science. *arXiv preprint arXiv:2502.13107*, 2025.

Taori, R., Gulrajani, I., Zhang, T., Dubois, Y., Li, X., Guestrin, C., Liang, P., and Hashimoto, T. B. Alpaca: A strong, replicable instruction-following model. *Stanford Center for Research on Foundation Models. https://crfm.stanford.edu/2023/03/13/alpaca.html*, 3(6):7, 2023.

Taylor, R., Kardas, M., Cucurull, G., Scialom, T., Hartshorn, A., Saravia, E., Poulton, A., Kerkez, V., and Stojnic, R. Galactica: A large language model for science. *arXiv preprint arXiv:2211.09085*, 2022.

Touvron, H., Martin, L., Stone, K., Albert, P., Almahairi, A., Babaei, Y., Bashlykov, N., Batra, S., Bhargava, P., Bhosale, S., et al. Llama 2: Open foundation and fine-tuned chat models. *arXiv preprint arXiv:2307.09288*, 2023.

Wang, C., Fan, H., Quan, R., and Yang, Y. Protchatgpt: Towards understanding proteins with large language models. *arXiv preprint arXiv:2402.09649*, 2024.

Wang, R., Yang, M., and Shen, Y. Bridging molecular graphs and large language models. In *Proceedings of the AAAI Conference on Artificial Intelligence*, volume 39, pp. 21234–21242, 2025a.

Wang, Z., Ma, Z., Cao, Z., Zhou, C., Zhang, J., and Gao, Y. Q. Prot2chat: protein large language model with early fusion of text, sequence, and structure. *Bioinformatics*, 41(8):btaf396, 2025b.

Xiao, Y., Sun, E., Jin, Y., Wang, Q., and Wang, W. Proteingpt: Multimodal llm for protein property prediction and structure understanding. *arXiv preprint arXiv:2408.11363*, 2024a.

Xiao, Y., Sun, E., Jin, Y., and Wang, W. Rna-gpt: Multi-modal generative system for rna sequence understanding. *arXiv preprint arXiv:2411.08900*, 2024b.

Xu, C., Guo, D., Duan, N., and McAuley, J. Baize: An open-source chat model with parameter-efficient tuning on self-chat data. *arXiv preprint arXiv:2304.01196*, 2023a.

Xu, M., Yuan, X., Miret, S., and Tang, J. Protst: Multi-modality learning of protein sequences and biomedical texts. In *International Conference on Machine Learning*, pp. 38749–38767. PMLR, 2023b.

Yan, M., Yu, Y., Zhang, R., Liu, Z., Zhang, R., Ren, Y., Lu, K., Huang, Z., Luo, F., and Cai, Z. Deepmoltex: Deep alignment of molecular graphs with large language models via mixture of modality experts. In *Proceedings of the 33rd ACM International Conference on Multimedia*, pp. 2323–2332, 2025.

Yang, A., Li, A., Yang, B., Zhang, B., Hui, B., Zheng, B., Yu, B., Gao, C., Huang, C., Lv, C., et al. Qwen3 technical report. *arXiv preprint arXiv:2505.09388*, 2025a.

Yang, Z., Chen, Y., Xie, J., Gao, B., Shen, S., Liu, W., Yang, L., Wang, B., Fu, T., and Li, Y. Molact: An agentic rl framework for molecular editing and property optimization. *arXiv e-prints*, pp. arXiv–2512, 2025b.

Zhang, O., Zhang, X., Lin, H., Tan, C., Wang, Q., Mo, Y., Feng, Q., Du, G., Yu, Y., Jin, Z., et al. Odesign: A world model for biomolecular interaction design. *arXiv preprint arXiv:2510.22304*, 2025a.

Zhang, Y., Guo, Q., Chen, Q., Zhang, L., Cui, H., and Chen, X. Llm3-dti: A large language model and multi-modal data co-powered framework for drug-target interaction prediction. *arXiv preprint arXiv:2511.06269*, 2025b.

Zheng, L., Chiang, W.-L., Sheng, Y., Zhuang, S., Wu, Z., Zhuang, Y., Lin, Z., Li, Z., Li, D., Xing, E., Zhang, H., Gonzalez, J. E., and Stoica, I. Judging llm-as-a-judge with mt-bench and chatbot arena. *ArXiv*, abs/2306.05685, 2023.

Zhuo, L., Chi, Z., Xu, M., Huang, H.-Y., Zhao, J., Zheng, H., He, C., Mao, X.-L., and Zhang, W. Protllm: An interleaved protein-language llm with protein-as-word pre-training. In *Proceedings of the 62nd Annual Meeting of the Association for Computational Linguistics (Volume 1: Long Papers)*, pp. 8950–8963, 2024.

Appendix Table of Contents

A. Theoretical Analysis and Proofs

- A.1 Gradient Correctness of Complexity-Aware Patching
- A.2 Mutual-Information Perspective on Instruction-Conditioned Fusion
- A.3 Definitions on Scaling and Modality Scope

B. Related Literature Review

- B.1 Structure LLMs: From Sequence Supervision to Structure Grounding
- B.2 The Development of All-Atom Modeling
- B.3 Q-Former Development and Widespread Use
- B.4 Recurring Limitations Across Prior Designs

C. Implementation Details

- C.1 Hyperparameter and Settings
- C.2 Data Process
- C.3 Encoder Pretraining Data
- C.4 Masked Reasoning Augmentation for Improved Latent Deliberation

D. Experiment Details

- D.1 Datasets and Benchmarks
- D.2 Baselines
- D.3 Benchmark Metrics
- D.4 Detailed Benchmark Results
- D.5 Reasoning Cases
- D.6 Data Contamination Analysis
- D.7 Training Efficiency Analysis

E. Extended Ablations

- E.1 Effect of Backbone Model Size
- E.2 Effect of LLM Adaptation Epochs
- E.3 Pooling Strategy for Patch Aggregation
- E.4 Maximum Patch Count
- Effect of Training Stages

F. Limitations and Future Work

- F.1 Limitations
- F.2 Future Work

G. Reproducibility

A. Theoretical Analysis and Proofs

A.1. Gradient Correctness of Complexity-Aware Patching

This section shows that the gate $g_{\text{anc}}(\cdot)$ and the soft patch growth and pooling operations in Alg. 1 admit well-defined gradients, and that reverse-mode automatic differentiation returns the exact derivatives of the executed computation graph. All symbols follow Alg. 1.

Preliminaries and Notation Fix one forward pass with instruction embeddings $\mathbf{z} \in \mathbb{R}^{G \times D_{\text{LLM}}}$, node embeddings $\mathbf{X} \in \mathbb{R}^{N \times D_{\text{enc}}}$, coordinates $\mathbf{P} \in \mathbb{R}^{N \times 3}$, and batch assignment $\mathbf{b} \in \{0, \dots, G-1\}^N$. For each graph index $g \in \{0, \dots, G-1\}$, define the node set

$$\mathcal{I}_g \triangleq \{i \mid \mathbf{b}_i = g\}. \quad (7)$$

Alg. 1 outputs patch tokens \mathbf{T} , mask \mathbf{M} , and anchor indices \mathbf{A} . Consider a scalar objective

$$\mathcal{L} = \mathcal{L}(\mathbf{T}, \mathbf{M}, \mathbf{A}, (\text{downstream outputs})). \quad (8)$$

We study gradients with respect to $(\mathbf{z}, \mathbf{X}, \mathbf{P})$ and the parameters of g_{anc} .

Step 1: Instruction-Conditioned Anchor Scoring Has Gradients Alg. 1 first computes

$$\boldsymbol{\ell} \leftarrow g_{\text{anc}}(\mathbf{z}, \mathbf{X}, \mathbf{b}), \quad \boldsymbol{\ell} \in \mathbb{R}^N. \quad (9)$$

Model form (as implemented). The implementation applies an MLP pointwise to the concatenation of each node embedding and its graph instruction vector:

$$\mathbf{u}_i \triangleq \mathbf{z}_{\mathbf{b}_i}, \quad \mathbf{h}_i \triangleq [\mathbf{X}_i; \mathbf{u}_i], \quad \boldsymbol{\ell}_i \triangleq \text{MLP}(\mathbf{h}_i). \quad (10)$$

The MLP uses affine maps, SiLU, and dropout. For a fixed dropout mask, dropout is piecewise differentiable in its input, and at evaluation it is the identity.

Lemma A.1 (Differentiability of g_{anc}). *For any fixed dropout mask, the mapping $(\mathbf{z}, \mathbf{X}) \mapsto \boldsymbol{\ell} = g_{\text{anc}}(\mathbf{z}, \mathbf{X}, \mathbf{b})$ is everywhere differentiable, and the Jacobians $\partial \boldsymbol{\ell} / \partial \mathbf{z}$ and $\partial \boldsymbol{\ell} / \partial \mathbf{X}$ exist and are finite.*

Proof. Each $\boldsymbol{\ell}_i$ is a composition of concatenation, affine maps, and $\text{SiLU}(t) = t\sigma(t)$, which is smooth. The gather $\mathbf{z}_{\mathbf{b}_i}$ is linear in \mathbf{z} for fixed \mathbf{b} . Therefore g_{anc} is differentiable in (\mathbf{z}, \mathbf{X}) with finite Jacobians.

Gradient correctness. Since g_{anc} is a composition of differentiable primitives for a fixed dropout mask, reverse-mode autodiff returns the exact gradient of the executed computation with respect to all inputs and parameters.

Step 2: Mass-Based Anchor Selection Is Discrete but Has Correct Piecewise Gradients For each g , the anchor set is selected via softmax probabilities and a cumulative-mass threshold:

$$\mathbf{p} \leftarrow \text{Softmax}(\boldsymbol{\ell}_{\mathcal{I}_g}), \quad \pi \leftarrow \text{Argsort}(\mathbf{p}), \quad k_g \leftarrow \min\left(K_{\text{max}}, \min\{k : \sum_{j=1}^k \mathbf{p}_{\pi_j} \geq \rho\}\right), \quad \mathcal{S}_g \leftarrow \{\mathcal{I}_g[\pi_1], \dots, \mathcal{I}_g[\pi_{k_g}]\}. \quad (11)$$

The map $\boldsymbol{\ell}_{\mathcal{I}_g} \mapsto \mathcal{S}_g$ is discrete because of sorting and thresholding, hence it is not globally differentiable.

Define the boundary set where ties occur or the threshold is met exactly:

$$\mathcal{B}_g \triangleq \left\{ \boldsymbol{\ell}_{\mathcal{I}_g} : \exists a \neq a' \text{ s.t. } \mathbf{p}_a = \mathbf{p}_{a'} \right\} \cup \left\{ \boldsymbol{\ell}_{\mathcal{I}_g} : \exists k \text{ s.t. } \sum_{j=1}^k \mathbf{p}_{\pi_j} = \rho \right\}. \quad (12)$$

If $\boldsymbol{\ell}_{\mathcal{I}_g} \notin \mathcal{B}_g$, then π and \mathcal{S}_g are locally constant, so subsequent steps execute on fixed indices.

Proposition A.2 (Piecewise gradient correctness through discrete selection). *Fix g and assume $\boldsymbol{\ell}_{\mathcal{I}_g} \notin \mathcal{B}_g$ so that \mathcal{S}_g is locally constant. For any downstream scalar loss \mathcal{L} depending on \mathbf{T} , backpropagation through the executed Steps 3 and 4 returns the classical gradient of \mathcal{L} with respect to $(\mathbf{z}, \mathbf{X}, \mathbf{P}, \{\boldsymbol{\ell}_a\}_{a \in \mathcal{S}_g})$, and $\partial \mathcal{L} / \partial \boldsymbol{\ell}_i = 0$ for $i \notin \mathcal{S}_g$ within that neighborhood.*

Proof. With \mathcal{S}_g fixed, Steps 3 and 4 are compositions of smooth maps plus linear gather and scatter with fixed indices. Hence \mathcal{L} is differentiable in the executed continuous variables, and reverse-mode autodiff returns the exact classical gradient of that smooth composition. Variables unused by the executed graph have zero partial derivatives.

Step 3: Soft Assignment Patch Growth Is Smooth For each $g, i \in \mathcal{I}_g$, and $a \in \mathcal{S}_g$, define squared distances, scores, and soft assignments:

$$\mathbf{D}_{i,a} \triangleq \|\mathbf{P}_i - \mathbf{P}_a\|_2^2, \quad \mathbf{S}_{i,a} \triangleq -\mathbf{D}_{i,a} + \ell_a, \quad \mathbf{W}_{i,:} \triangleq \text{Softmax}_a(\mathbf{S}_{i,:}). \quad (13)$$

Lemma A.3 (Softmax Jacobian). *For fixed i , $\mathbf{S}_{i,:} \mapsto \mathbf{W}_{i,:}$ is smooth with*

$$\frac{\partial \mathbf{W}_{i,a}}{\partial \mathbf{S}_{i,a'}} = \mathbf{W}_{i,a} (\delta_{a,a'} - \mathbf{W}_{i,a'}). \quad (14)$$

Lemma A.4 (Gradients of distances and anchor bias). *For each (i, a) ,*

$$\frac{\partial \mathbf{D}_{i,a}}{\partial \mathbf{P}_i} = 2(\mathbf{P}_i - \mathbf{P}_a), \quad \frac{\partial \mathbf{D}_{i,a}}{\partial \mathbf{P}_a} = 2(\mathbf{P}_a - \mathbf{P}_i), \quad \frac{\partial \mathbf{S}_{i,a}}{\partial \ell_a} = 1. \quad (15)$$

Conclusion for Step 3. Conditioned on fixed \mathcal{S}_g , \mathbf{W} is smooth in $(\mathbf{P}_{\mathcal{I}_g}, \mathbf{P}_{\mathcal{S}_g}, \{\ell_a\}_{a \in \mathcal{S}_g})$, with gradients given by chaining (14) and (15).

Step 4: Patch Token Pooling Is Differentiable The implementation normalizes weights per anchor across nodes. Define

$$m_a \triangleq \sum_{i \in \mathcal{I}_g} \mathbf{W}_{i,a} + \varepsilon, \quad \widetilde{\mathbf{W}}_{i,a} \triangleq \mathbf{W}_{i,a}/m_a, \quad \mathbf{T}_a \triangleq \sum_{i \in \mathcal{I}_g} \widetilde{\mathbf{W}}_{i,a} \mathbf{X}_i \in \mathbb{R}^{D_{\text{enc}}}, \quad \varepsilon > 0. \quad (16)$$

Lemma A.5 (Pooling gradients). *Fix g and $a \in \mathcal{S}_g$. The map $(\mathbf{X}_{\mathcal{I}_g}, \mathbf{W}_{\mathcal{I}_g, a}) \mapsto \mathbf{T}_a$ is differentiable, and for each $i \in \mathcal{I}_g$,*

$$\frac{\partial \mathbf{T}_a}{\partial \mathbf{X}_i} = \widetilde{\mathbf{W}}_{i,a} \mathbf{I}_{D_{\text{enc}}}, \quad \frac{\partial \mathbf{T}_a}{\partial \mathbf{W}_{i,a}} = \frac{1}{m_a} (\mathbf{X}_i - \mathbf{T}_a). \quad (17)$$

Proof. Since $m_a \geq \varepsilon > 0$, $\widetilde{\mathbf{W}}_{i,a}$ is differentiable in $\mathbf{W}_{:,a}$. The first identity follows from linearity in \mathbf{X}_i . For the second, write $\mathbf{T}_a = (1/m_a) \sum_{j \in \mathcal{I}_g} \mathbf{W}_{j,a} \mathbf{X}_j$ and apply the quotient rule.

Conclusion for Step 4. Gradients propagate from \mathcal{L} to \mathbf{X} via a linear map and to \mathbf{W} , hence to \mathbf{P} and ℓ , via differentiable normalization and pooling.

Main Theorem: Correct Gradients for \mathbf{T} Almost Everywhere

Theorem A.6 (Gradient existence and correctness). *Fix a forward pass of Alg. 1. Consider the map $(\mathbf{z}, \mathbf{X}, \mathbf{P}) \mapsto \mathbf{T}$ produced by Steps 1 to 4.*

1. *Conditioned on $\{\mathcal{S}_g\}_{g=0}^{G-1}$, the map is differentiable, with derivatives obtained by chaining (9), (14), (15), and (17).*
2. *The only non-differentiabilities arise from the discrete selection in (11) and any optional discrete truncations. Hence the overall map is piecewise smooth. Outside the boundary sets (12), $\{\mathcal{S}_g\}$ is locally constant and the gradient equals the gradient of the conditioned smooth computation.*
3. *Reverse-mode autodiff returns the exact gradient of the executed computation graph. In particular, it returns the classical gradient holding the realized $\{\mathcal{S}_g\}$ fixed, and gradients flow to the parameters of g_{anc} through the anchor bias in (13) for anchors $a \in \mathcal{S}_g$.*

Proof. With $\{\mathcal{S}_g\}$ fixed, Step 1 is differentiable by Lem. A.1, and Steps 3 and 4 are compositions of smooth primitives and linear gathers and scatters with fixed indices, using Lem. A.3, Lem. A.4, and Lem. A.5. This yields item (1) by the chain rule. Item (2) follows because (11) is locally constant off (12), and the boundary has Lebesgue measure zero in $\mathbb{R}^{|\mathcal{I}_g|}$. Item (3) follows from the exactness of reverse-mode autodiff on the executed smooth subgraph with indices treated as constants.

Remarks on Correct Gradients Through Discrete Steps Step 2 realizes a complexity-aware anchor count via ρ and K_{\max} . The returned gradient is the correct gradient of the executed computation, namely the gradient within the current piecewise-smooth region with $\{\mathcal{S}_g\}$ held fixed. It does not directly optimize the discrete choice of $\{\mathcal{S}_g\}$.

Corollary: End-to-End Differentiability of the Fusion Stack In the reference implementation, \mathbf{T} is processed by standard cross-attention fusion blocks composed of layer normalization, multi-head attention, feed-forward layers, residual connections, and pointwise nonlinearities such as GELU. These operators are differentiable, so once gradients to \mathbf{T} exist as above, gradients propagate end to end through the fusion stack and into $(\mathbf{z}, \mathbf{X}, \mathbf{P})$ and the parameters of g_{anc} .

A.2. Mutual-Information Perspective on Instruction-Conditioned Fusion

This section casts the fusion flow as an instruction-conditioned information bottleneck: the gate and patcher compress (\mathbf{X}, \mathbf{P}) into budgeted tokens (\mathbf{T}, \mathbf{M}) aligned with \mathbf{z} , and cross-attention reads out task-relevant information into the LLM.

Problem setup. Let $\mathbf{z} \in \mathbb{R}^{G \times D_{\text{LLM}}}$ be instruction embeddings, $\mathbf{X} \in \mathbb{R}^{N \times D_{\text{enc}}}$ node embeddings, $\mathbf{P} \in \mathbb{R}^{N \times 3}$ coordinates, and $\mathbf{b} \in \{0, \dots, G-1\}^N$ the batch assignment. Let $g_{\text{anc}}(\cdot)$ be the anchor gate with maximum anchors K_{\max} and mass threshold ρ . Patching outputs tokens $\mathbf{T} \in \mathbb{R}^{G \times K \times D_{\text{enc}}}$, mask $\mathbf{M} \in \{0, 1\}^{G \times K}$, and anchor indices $\mathbf{A} \in \{1, \dots, N\}^{G \times K}$. For fusion, let $\mathbf{E} \in \mathbb{R}^{B \times L \times D_{\text{LLM}}}$ be LLM embeddings, $\{f_\ell\}_{\ell=1}^{L_f}$ fusion blocks, and y_{ins} the modality placeholder id.

Mutual-information view. The fusion instantiates an instruction-conditioned information bottleneck from (\mathbf{X}, \mathbf{P}) to the LLM via (\mathbf{T}, \mathbf{M}) :

$$\ell = g_{\text{anc}}(\mathbf{z}, \mathbf{X}, \mathbf{b}), \quad p(\mathbf{A} \mid \mathbf{z}, \mathbf{X}, \mathbf{b}) := \text{Select}_{(K_{\max}, \rho)}(\ell), \quad (\mathbf{T}, \mathbf{M}) = (\phi(\mathbf{X}, \mathbf{P}, \mathbf{A}, \mathbf{b}), \psi(\mathbf{A}, \mathbf{b})). \quad (18)$$

Fusion is a deterministic readout

$$\mathbf{E}' = (f_{L_f} \circ \dots \circ f_1)(\mathbf{E}, \mathbf{T}, \mathbf{M}, y_{\text{ins}}). \quad (19)$$

Lemma 1 (Budgeted, instruction-aligned compression). Let random variables (Z, X) induce a joint distribution (with Z representing the instruction). Let $A \sim p(A \mid Z, X, \mathbf{b})$ be a (possibly stochastic) selector constrained by (K_{\max}, ρ) , and let $T = \phi(X, \mathbf{P}, A, \mathbf{b})$ be deterministic. A natural objective for selector design under a strict token budget is to maximize instruction alignment of the retained representation:

$$\max_{p(A \mid Z, X, \mathbf{b})} I(Z; T) \quad \text{s.t.} \quad |A| \leq K_{\max}, \text{ mass}(A) \geq \rho. \quad (20)$$

Moreover, for any variational decoder $q_\eta(z \mid t)$,

$$I(Z; T) = \mathbb{E}[\log p(z \mid t) - \log p(z)] \geq \mathbb{E}[\log q_\eta(z \mid t)] + H(Z). \quad (21)$$

Proof sketch. The lower bound (21) follows by substituting $q_\eta(z \mid t)$ for $p(z \mid t)$ and applying $\text{KL}(p(\cdot \mid t) \parallel q_\eta(\cdot \mid t)) \geq 0$. Under fixed (K_{\max}, ρ) , increasing $\mathbb{E}[\log q_\eta(Z \mid T)]$ increases a certified lower bound on $I(Z; T)$. In our construction, A is explicitly instruction-conditioned via $\ell = g_{\text{anc}}(\mathbf{z}, \mathbf{X}, \mathbf{b})$ in (18), while $\text{Select}_{(K_{\max}, \rho)}$ enforces the bottleneck.

Lemma 2 (Fusion is an information-preserving readout of the bottleneck). Let Y be the desired output text or labels for the same sample. Since \mathbf{E}' is a deterministic function of $(\mathbf{E}, \mathbf{T}, \mathbf{M})$ given Z by (19), the data processing inequality yields

$$I(Y; \mathbf{E}' \mid Z) \leq I(Y; (\mathbf{E}, \mathbf{T}, \mathbf{M}) \mid Z). \quad (22)$$

Thus, any increase in $I(Y; \mathbf{E}' \mid Z)$ must be realized by extracting task-relevant information already present in $(\mathbf{E}, \mathbf{T}, \mathbf{M})$, which is exactly the role of cross-attention fusion blocks $\{f_\ell\}$.

Furthermore, for any predictor $p_\theta(y \mid \mathbf{E}')$ (LLM head), the conditional mutual information admits the standard variational bound

$$I(Y; T \mid Z) = H(Y \mid Z) - H(Y \mid T, Z) \geq H(Y \mid Z) + \mathbb{E}[\log p_\theta(Y \mid \mathbf{E}')]. \quad (23)$$

Proof sketch. The inequality (23) follows from $-H(Y \mid T, Z) = \mathbb{E}[\log p(y \mid t, z)] \geq \mathbb{E}[\log p_\theta(y \mid \mathbf{E}')]$, since \mathbf{E}' is a (deterministic) function of (\mathbf{E}, T, M, Z) by (19) and $\text{KL}(p(\cdot \mid t, z) \parallel p_\theta(\cdot \mid \mathbf{E}')) \geq 0$. Therefore maximizing the log-likelihood term $\mathbb{E}[\log p_\theta(Y \mid \mathbf{E}')]$ via cross-entropy training increases a lower bound on $I(Y; T \mid Z)$.

Table 8. Comparison of All-Atom Models for Protein Structure and Molecular Design. Representative works are categorized by their architectural intent, including structural representation, generative design, and LLM-guided optimization.

Model / Paper	What it does	Category
AlphaFold1 (Senior et al., 2020)	End-to-end protein structure prediction	Structural ML
AlphaFold2 (Jumper et al., 2021)	Near-experimental protein folding at scale	Structural ML
AlphaFold3 (Abrams et al., 2024)	Joint prediction of biomolecular interactions	Structural foundation model
ATOMICA (Fang et al., 2025)	Universal atom-level interaction representations	Structural representation model
ODesign (Zhang et al., 2025a)	World-model for interaction-driven design	Structural generative model
BoltzGen (Stark et al., 2025)	Generative universal protein binder design	Binder generative model
All-atom Diffusion Transformers (Joshi et al., 2025)	Unified atomistic diffusion modeling	Structural foundation model
MolAct (Yang et al., 2025b)	Agent-based molecular editing and optimization	Molecular agent model
CIDD (Gao et al., 2025)	LLM-guided structure-based drug design	Structure-grounded LLM

Theorem (Mutual-information consistency of the fusion flow). The pipeline implements an instruction-conditioned information bottleneck

$$(\mathbf{X}, \mathbf{P}) \xrightarrow[\left(K_{\max}, \rho \right)]{g_{\text{anc}}, \phi, \psi} (\mathbf{T}, \mathbf{M}) \xrightarrow{\{f_{\ell}\}} \mathbf{E}' \xrightarrow{\text{LLM head}} \hat{Y}. \quad (24)$$

By Lemma 1, gating and patching perform a budgeted compression that increases a certified lower bound on $I(Z; T)$, aligning the retained modality evidence with the instruction. By Lemma 2, fusion and likelihood training increase a certified lower bound on $I(Y; T | Z)$, encouraging T to carry task-relevant modality information conditioned on Z and making it retrievable into \mathbf{E}' at the placeholder y_{ins} . Hence the anchor-patch bottleneck followed by cross-attention fusion is mutual-information consistent: it preserves instruction-relevant modality information under a strict token budget and exposes that information to the LLM through a principled readout that aligns with maximizing task likelihood.

A.3. Definitions on Scaling and Modality Scope

Scaling Definition (Entity Complexity). In this paper, **scaling** denotes **all-atom entity complexity scaling, defined directly by the atom count N_{atom} of the input entity**. We do not study backbone scaling (e.g., parameter count, depth) and do not attribute scaling effects to increasing LLM capacity. Scaling arises from larger structural entities containing more atoms and thus richer local environments and long-range relations. When structural inputs are tokenized, the resulting structural token count is a consequence of N_{atom} , not the definition of scaling.

Scope of “Molecules”. In this work, the term **molecules refers to small-molecule chemical entities**, including drug-like compounds, ligands, metabolites, and related low-molecular-weight species. These entities are characterized by moderate atom counts and well-defined stereochemistry. Large macromolecules are explicitly excluded from this category; in particular, proteins and nucleic acids are not treated as molecules for scaling or evaluation purposes in this paper.

Scope of “Proteins”. The **protein modality encompasses a broad granularity range**, including short peptides, partial protein sequences or domains, and full-length functional proteins. Scaling within this modality reflects variations in amino-acid length and corresponding all-atom representations, while remaining within the biochemical definition of proteins.

DNA and RNA Structures. For nucleic acids, we consider only **sequence-derived all-atom structures** that are directly displayed from linear DNA or RNA sequences. Higher-order folding phenomena occurring in the cellular nucleus or cytoplasm are not modeled. This design choice is motivated by: (i) the extreme complexity and context-dependence of in vivo nucleic-acid folding, which is beyond the scope of unified all-atom learning; (ii) the objective of maintaining a consistent structural abstraction across modalities; and (iii) the empirical observation that nucleic acids are not the primary performance driver of the proposed framework. The modest yet consistent improvements observed on DNA/RNA benchmarks support the feasibility of this simplified representation, while full nucleic-acid folding is left for future investigation.

B. Related Literature Review

This appendix complements the main-text related work and summarizes it as Tab. 8 and Tab. 9. This section emphasizes two threads: structure-grounded biology LLMs organized by fusion strategy, and recent atom-level structural foundation and generative models that demonstrate feasible all-atom scaling.

B.1. Structure LLMs: From Sequence Supervision to Structure Grounding

Modality scope. Prior biology LLMs span molecules, proteins, and nucleic acids, with parallel development patterns across modalities. Molecular systems cover representation alignment, captioning, reasoning, and instruction following; protein systems extend from sequence alignment to open-ended dialogue and structure-conditioned interaction; nucleic-acid systems include unified DNA and RNA modeling and RNA-focused instruction tuning.

Integration strategies. Existing approaches can be organized by how structural information is exposed to the language model. **(i) Sequence-only modeling.** Several baselines rely on sequence inputs without explicit structural grounding, including MolT5 (Edwards et al., 2022) for molecules, ProtST (Xu et al., 2023b) for proteins, RNA-GPT (Xiao et al., 2024b) for nucleic acids, and ChatNT (de Almeida et al., 2025) via sequence concatenation across complex. This line prioritizes language modeling convenience but leaves geometry implicit.

(ii) Embedding-only alignment. Contrastive co-embedding methods align molecular structure and text for retrieval and editing (MoleculeSTM (Liu et al., 2023b), MoMu (Su et al., 2022)), and similar embedding-only modeling appears for drug target interaction (LLM3-DTI (Zhang et al., 2025b)). These methods provide strong alignment primitives yet do not directly instantiate token-level structural reasoning.

(iii) Fixed-length projection and feature injection. A common design projects encoder outputs into a fixed token budget, as in InstructMol (Cao et al., 2025) and Chem3DLM (Jiang et al., 2025), or injects encoder features into prompts, as in ProteinGPT (Guo et al., 2023). These designs are simple and effective, but they enforce constant-capacity structure summaries.

(iv) Q-Former-style query connectors and variants. Many models adopt fixed-length query tokens that attend to encoder representations, producing a small set of modality anchors. This connector pattern appears in molecular settings (GIT-Mol (Liu et al., 2023a), 3D-MoLM (Li et al., 2024), UniMoT (Guo et al., 2025b), MolCA (Liu et al., 2023c)), protein dialogue settings (ProtChatGPT (Wang et al., 2024)), and materials QA (MatterChat (Tang et al., 2025)), with instruction-conditioned variants (Prot2Chat (Wang et al., 2025b), LLaMo (Park et al., 2024)) and multi-stream extensions. In parallel, cross-attention bridges can be framed as tokenizing structural embeddings through attention, as in Graph2Token (Wang et al., 2025a). DeepMolTex (Yan et al., 2025) extends projection fusion with multi-scale projectors spanning atom, motif, and molecule representations, still under a fixed-length fusion regime.

B.2. The Development of All-Atom Modeling

A distinct, rapidly maturing line demonstrates that atom-resolved modeling can scale to realistic biomolecular complexity (Tab. 8). Structural ML and structural foundation models progress from protein folding at scale (AlphaFold (Senior et al., 2020), AlphaFold2 (Jumper et al., 2021)) to joint biomolecular interaction prediction (AlphaFold3 (Abramson et al., 2024)). Atom-level representation and generative modeling further expand the capability envelope, including universal atom-level interaction representations (ATOMICA (Fang et al., 2025)), interaction-driven world-model design (ODesign (Zhang et al., 2025a)), binder design (BoltzGen (Stark et al., 2025)), and unified atomistic diffusion modeling (All-atom Diffusion Transformers). Complementary directions connect atom-level structure to downstream design and optimization pipelines, including agent-based molecular editing (MolAct (Yang et al., 2025b)), LLM-guided structure-based drug design (CIDD (Gao et al., 2025)).

Collectively, these results motivate an all-atom perspective for language grounding: atom-resolved representations are now practical, and generative models can operate at atomistic resolution, suggesting a viable path to move beyond residue-level abstractions in structure-grounded LLMs.

B.3. Q-Former Development and Widespread Use

Q-Former-style connectors operationalize cross-modal grounding by introducing a fixed set of learnable query tokens that attend to modality encoder outputs, producing a compact token sequence consumable by an LLM (Li et al., 2023). In the biology and chemistry literature summarized in Tab. 9, this mechanism is repeatedly adopted as a general-purpose fusion layer, spanning molecules (GIT-Mol (Liu et al., 2023a), 3D-MoLM (Li et al., 2024), UniMoT (Consortium, 2019), MolCA (Liu et al., 2023c), LLaMo (Park et al., 2024)), proteins (ProtChatGPT (Wang et al., 2024), Prot2Chat (Wang et al., 2025b)), and even materials (MatterChat (Tang et al., 2025)). The prevalence of this pattern reflects two practical advantages: architectural modularity and compatibility with instruction tuning while maintaining an LLM-native token interface.

Table 9. Comparison of Structure-Grounded Foundation Models categorized by Domain and Fusion Strategy. The models are organized into five primary domains based on the chemical entity they represent: Molecular LLMs, Protein LLMs, Nucleic Acid LLMs, and Materials LLMs focus on generative or reasoning tasks, while Embedding Models prioritize latent-space alignment for retrieval.

Model	Core Idea	Category	Fusion
MoleculeSTM (Liu et al., 2023b)	Contrastive alignment between molecular structures and text for retrieval and text-guided molecular editing	Molecular Embedding	Embedding only
MoMu (Su et al., 2022)	Contrastive graph–text alignment supporting retrieval and molecular captioning	Molecular LLM	Fixed length projection fusion
MolT5 (Pei et al., 2024)	Sequence based molecular text generation without explicit structural grounding	Molecular LLM	Sequence only
InstructMol (Cao et al., 2025)	Instruction tuned molecular reasoning with graph encoders aligned to text	Molecular LLM	Fixed length projection fusion
GIT-Mol (Liu et al., 2023a)	Adapter-based instruction following over sequence, graph, and image modalities	Molecular LLM	Fixed-length Q-Former style connector
3D-MoLM (Li et al., 2024)	Q-Former queries attending to 3D molecular representations from structure encoders	Molecular LLM	Fixed length Q-Former style connector
UniMoT (Guo et al., 2025b)	Unified molecular tokenizer for sequences with Q-Former based structural grounding	Molecular LLM	Fixed length Q-Former style connector
Graph2Token (Wang et al., 2025a)	Graph–text bridge using cross attention to convert graph embeddings into token representations	Molecular LLM	Fixed length cross attention fusion
MolCA (Liu et al., 2023c)	Joint modeling of molecular sequence and structure via Q-Former alignment	Molecular LLM	Fixed length Q-Former style connector
LLaMo (Park et al., 2024)	Multi-stream integration of sequence, graph tokens, and instructions for molecular reasoning	Molecular LLM	Fixed length multi-stream Q-Former connector
DeepMolTex (Yan et al., 2025)	Multi-scale graph projectors aligning atom, motif, and molecule representations with text	Molecular LLM	Fixed length multi-stream projection fusion
ProtST (Xu et al., 2023b)	Contrastive alignment between protein sequences and textual descriptions	Protein LLM	Sequence only
ProtLLM (Zhuo et al., 2024)	Protein sequence encoding followed by text fusion for language modeling	Protein LLM	Sequence concatenation fusion
Prot2Text-V2 (Fei et al., 2025)	Encoder-based protein sequence representation fused with text for generation	Protein LLM	Sequence concatenation fusion
ProteinGPT (Xiao et al., 2024a)	Injection of protein sequence and structure features into LLM prompts with instruction tuning	Protein LLM	Encoder feature injection
ProtChatGPT (Wang et al., 2024)	Instruction guided protein chat with structural embedding grounding	Protein LLM	Fixed length Q-Former style connector
Chem3DLM (Jiang et al., 2025)	Structure–text fusion for protein reasoning using learned projections	Protein LLM	Fixed length projection fusion
Prot2Chat (Wang et al., 2025b)	Instruction guided adapters integrating protein structure and text	Protein LLM	Fixed length instruction conditioned Q-Former connector
ChatNT (de Almeida et al., 2025)	Unified grounding of DNA, RNA, and protein sequences for language modeling	Nucleic Acid LLM	Sequence concatenation fusion
RNA-GPT (Xiao et al., 2024b)	Instruction-tuned RNA sequence modeling without explicit structural input	Nucleic Acid LLM	Sequence only
LLM3-DTI (Zhang et al., 2025b)	Multimodal modeling of topology graphs and text for drug–target interaction	Embedding Model	Embedding only
DrugAgent (Inoue et al., 2025)	Multi-agent LLM framework for drug–target interaction with planning and tool use	Agent System	LLM as planner and evaluator
MatterChat (Tang et al., 2025)	Atom resolved structure grounded question answering for materials science	Materials LLM	Fixed length Q-Former style connector

B.4. Recurring Limitations Across Prior Designs

The models in Tab. 9 expose three recurring limitations that align with the main-text discussion.

Sequence-only under-species geometry. Sequence-only and sequence-concatenation approaches do not explicitly represent 3D structure, limiting structure-faithful understanding and generation when geometry is essential (MolT5 (Edwards et al., 2022), ProtST (Xu et al., 2023b), RNA-GPT (Xiao et al., 2024b), ChatNT (de Almeida et al., 2025)).

Table 10. Hyperparameters and configuration settings for Cuttlefish. The parameters specify the architectural dimensions for the graph encoder, the multimodal fusion blocks, and the spatial logic for the all-atom anchor assignment mechanism.

Parameter	Value	Parameter	Value	Parameter	Value
Graph encoder hidden size	256	Graph encoder depth	8	Graph encoder dropout	0.1
Coordinate updates	Enabled	Encoder LayerNorm	Enabled	Number of RBF bases	32
RBF cutoff distance	10.0	Fusion block count	8	Attention head count	32
Fusion model width	4096	Fusion MLP intermediate size	16384	Fusion dropout	0.1
Max anchors per graph	2048	Max nodes per anchor	None (soft pooling)	Mass-based anchor fraction	0.1
Assignment distance scale	1.0	Assignment temperature	0.1	Gate MLP hidden size	256

Table 11. Summary of training parameters used for modality alignment tuning. This includes the learning rate schedules, gradient accumulation strategies, etc., employed to optimize the multimodal integration between structural representations and the language model.

Parameter	Value	Parameter	Value	Parameter	Value
Base language model checkpoint	Llama-3.1-8B-Instruct	Optimizer	AdamW	Learning rate	1e-4
Training epochs	4	Per-device train batch size	1	Gradient accumulation steps	16
Warmup steps	100	Gradient clipping (max norm)	1.0	Weight decay	0.01
Adam beta1	0.9	Adam beta2	0.999	Adam epsilon	1e-8
Mixed precision (bf16)	Enabled	Gradient checkpointing	Enabled	Evaluation split ratio	0.1
Evaluation frequency (steps)	100	Logging frequency (steps)	10	DataLoader workers	8

Fixed-capacity connectors induce structural bottlenecks. Projection fusion and Q-Former-style connectors compress variable-size structures into a constant token budget (InstructMol (Cao et al., 2025), Chem3DLM (Jiang et al., 2025), Prot2Chat (Wang et al., 2025b), MatterChat (Tang et al., 2025)). This design choice constrains scalability with entity size and atom-level detail.

Tokenization bridges mitigate but do not remove capacity mismatch. Cross-attention tokenization, exemplified by Graph2Token (Wang et al., 2025a), reduces the gap between structural embeddings and language tokens, but it remains bounded by a fixed-length interface under increasing structural complexity.

These limitations motivate all-atom language grounding mechanisms that preserve fine geometry while allocating token budget adaptively with structural complexity, consistent with the framing in the main related-work section. Note that Agent works such as DrugAgent (Inoue et al., 2025), LLMs usually behave as a judge or planner, which is not in our context.

C. Implementation Details

This section details Cuttlefish implementation, covering architecture and optimization hyperparameters, modality-specific atom-level preprocessing with aligned 3D coordinates plus filtering and sequence-only fallbacks on rare structure failures, and masked reasoning augmentation that injects teacher-generated latent deliberation spans while applying loss only to final-answer tokens.

C.1. Hyperparameter and Settings

Model Configuration. Table 10 summarizes the core architecture hyperparameters of Cuttlefish, covering the graph encoder, the instruction-conditioned patching/assignment module, and the cross-attention fusion with the frozen LLM. The graph encoder hidden size and graph encoder depth specify the representation width and number of message-passing (equivariant) layers used to embed molecular/protein/nucleic-acid structures, with graph encoder dropout controlling regularization within this stack. Coordinate updates indicate whether the encoder performs equivariant coordinate refinement alongside feature updates, and encoder LayerNorm denotes the use of normalization for stabilizing deep message passing. The encoder’s geometric featurization is parameterized by the number of Radial Basis Function (RBF) bases and RBF cutoff distance, which define the resolution and range of radial basis embeddings for interatomic distances. For multimodal integration, fusion block count, attention head count, fusion model width, and fusion MLP intermediate size define the capacity of the cross-attention transformer blocks that align graph-derived tokens with the LLM embedding space, with fusion dropout providing additional regularization. Finally, the patching/assignment module is governed by max anchors per graph and max nodes per anchor, which control how graph nodes are grouped into anchor-based patches (with “None” indicating soft pooling without a hard cap), and mass-based anchor fraction, assignment distance scale, and assignment temperature, which shape the softness and selectivity of node-to-anchor assignments. Gate MLP hidden size specifies the width of the gating network that modulates connector behavior, enabling adaptive routing of structural information into the fusion pathway.

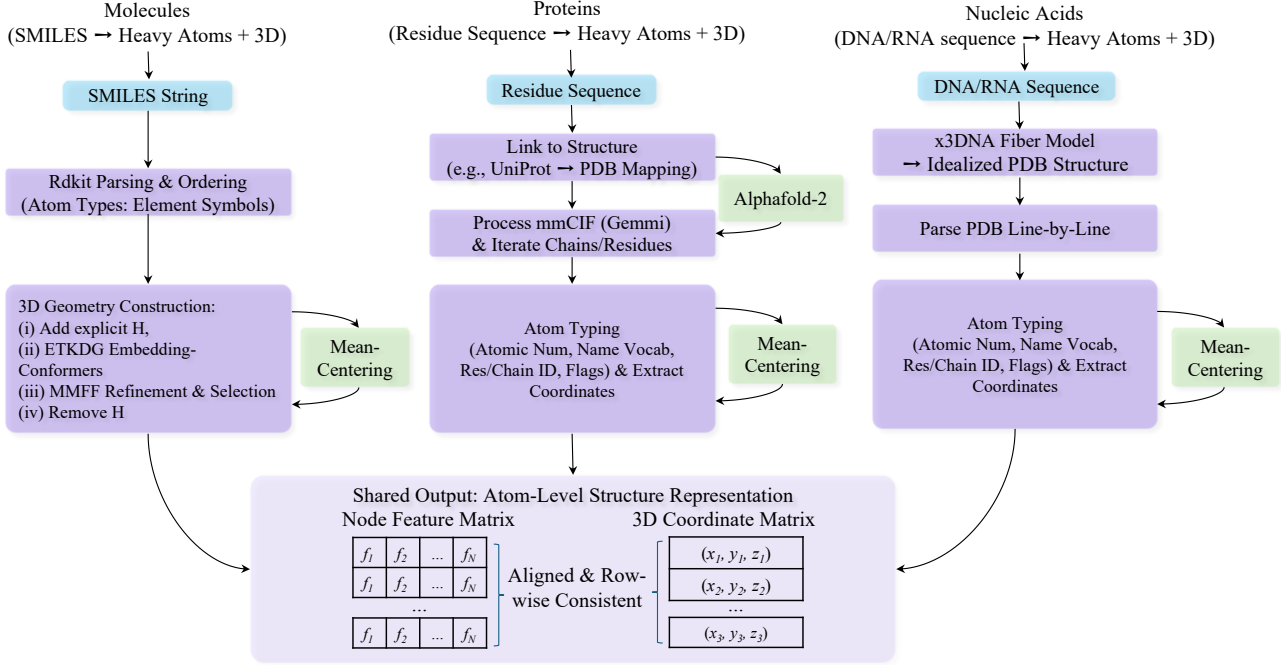


Figure 7. Multimodal structure generation and atom-level extraction. Three specialized streams process molecules (SMILES), proteins (residue sequences), and nucleic acids into a unified format. The pipeline ensures strict row-wise consistency between the atom-ordered node feature matrix and the aligned 3D coordinate matrix.

Training Configuration. Table 11 reports the main optimization and data-loading hyperparameters used in our two-stage tuning pipeline. In the modality alignment stage, we train the multimodal connector components with AdamW using a base learning rate of 1×10^{-4} , warmup, gradient accumulation, and gradient clipping for stability, together with bf16 and gradient checkpointing for memory efficiency. In the subsequent LLM adaptation stage, we keep the overall setup the same for fair comparison, but use a smaller learning rate (1×10^{-5}) than modality alignment to safely adapt the language model while avoiding destabilizing previously aligned multimodal representations.

C.2. Data Process

Structure generation and atom-level extraction. All modalities output (i) an atom-ordered node feature matrix and (ii) an aligned coordinate matrix $\mathbf{P} \in \mathbb{R}^{N \times 3}$ in Å, with strict row-wise consistency between atom typing, graph construction, and Cartesian positions. Fig. 7 illustrates the structure generation flow, described in the following paragraphs:

Molecules (SMILES → heavy atoms + 3D). SMILES parsed into an RDKit (Landrum, 2013) “Mol”; atom types defined as chemical element symbols in RDKit internal atom ordering. 3D geometry construction: (i) explicit hydrogen addition for embedding robustness, (ii) one or multiple conformer candidates via RDKit distance-geometry embedding (ETKDG), (iii) MMFF force-field refinement, best-conformer selection (typically lowest-energy converged). Post-selection hydrogen removal; returned $\mathbf{P} \in \mathbb{R}^{N \times 3}$ corresponds to the heavy-atom set and preserves the same atom order used for typing and graph building.

Proteins (residue sequence → matched PDB/mmCIF → atoms + 3D). Residue sequence linked to an experimental structure (e.g., UniProt↔PDB mapping or sequence search); corresponding mmCIF processed with Gemmi. Polymer chains and residues iterated; per-atom records extracted in parser-defined order. Atom typing encodes (1) atomic number from the element field and (2) atom-name vocabulary (e.g., N, CA, C, O, sidechain heavy atoms; unknown→“misc”), augmented by parent residue identity (3-letter residue vocabulary), chain index, residue index, and binary flags (e.g., `is_backbone`, `is_CA`). Coordinates taken directly from mmCIF atom positions (Å); optional mean-centering by subtracting the global coordinate mean. Feature rows and \mathbf{P} share identical atom ordering.

Table 12. Summary of proposed dataset GEO-AT: sources and counts by training stages and four modalities.

Stage	Modality	Source	Count
Encoder	Molecule	PubChem	1M
	Protein	UniProt	300K
	DNA	DNA-Chat	300K
	RNA	RNA-QA	200K
End-to-End	Molecule	MolLlama-Instruct	10K
	Protein	UniProt+PDB	10K
	DNA	DNA-Chat	5K
	RNA	RNA-QA	5K

A/C/G/U), chain and residue indices, and binary backbone and phosphate-group indicators. RNA follows the same pipeline, with alphabet $\{A, C, G, U\}$ and optional single-strand generation (default). Output coordinates $\mathbf{P} \in \mathbb{R}^{N \times 3}$ mean-centered by subtracting the coordinate mean; one-to-one alignment maintained between feature rows and coordinate rows.

Data filtering and fallbacks. Entities with invalid primary inputs were removed, including SMILES strings not parsable by RDKit (Landrum, 2013) and sequences failing modality-specific parsing. When sequence inputs were valid but 3D structure generation failed, samples were retained as sequence-only inputs to preserve coverage and ensure consistent, fair evaluation across models. This fallback occurred in fewer than 0.5% of cases and did not materially affect reported conclusions, including claims about structure-conditioned reasoning.

C.3. Encoder Pretraining Data

Following MuMo (Jing et al., 2025), samples are limited to the hundred-thousand scale, which suffices for representation convergence and feature alignment. For molecules, 1M samples from PubChem (Kim et al., 2023) are filtered by sequence length to cover structural complexity. 300K proteins from UniProt (Consortium, 2019) across key model organisms (Human, Mouse, Rat, A. thaliana, S. cerevisiae) are sampled. We include sequences with multiple conformers to capture structural flexibility. For nucleic acids, 300K DNA and 200K RNA samples from DNA-Chat (de Almeida et al., 2025) and RNA-QA (Xiao et al., 2024b). Data spans 30 functional categories across human and mouse genomes to ensure biological significance.

C.4. Masked Reasoning Augmentation for Improved Latent Deliberation

Motivation. Instruction tuning corpora for scientific QA and structured reasoning often provide only a final response label, without explicit intermediate rationales. Directly optimizing for short answer templates (for example, “The answer is A”) can bias training toward format memorization, reduce linguistic diversity, and degrade latent deliberation capacity. To mitigate this issue while avoiding the need for human reasoning annotations, masked reasoning augmentation is adopted.

Construction. As shown in Algo. 3, for each training instance with instruction x and gold final answer a , a teacher model (OpenAI GPT-5) produces a harmless and general reasoning span \tilde{r} . The span length is variable and may include placeholder style statements that indicate reasoning progress without encoding task-specific private labels. The final training target sequence is constructed as

$$y = [\langle \text{think} \rangle, \tilde{r}, \langle / \text{think} \rangle, a], \quad (25)$$

where $\langle \text{think} \rangle$ and $\langle / \text{think} \rangle$ are retained to delimit the latent deliberation region.

Masked objective. Let $y_{1:T}$ be the tokenization of y , and let $m_t \in \{0, 1\}$ denote a loss mask. The mask is set to exclude all tokens inside the reasoning span, while retaining supervision on the final answer tokens (and optionally the delimiter tokens):

$$m_t = \mathbb{1}[y_t \in a] \quad (\text{optionally } m_t \leftarrow 1 \text{ for delimiter tokens}). \quad (26)$$

Training minimizes a masked negative log likelihood:

$$\mathcal{L}(\theta) = -\mathbb{E}_{(x,a) \sim \mathcal{D}} \left[\sum_{t=1}^T m_t \log p_\theta(y_t | x, y_{<t}) \right]. \quad (27)$$

Algorithm 3 Masked Reasoning Augmentation

Input: Dataset $\mathcal{D} = \{(x^{(i)}, a^{(i)})\}_{i=1}^N$, teacher generator \mathcal{G} (GPT-5), model p_θ , delimiter tokens $\langle\text{think}\rangle, \langle/\text{think}\rangle$
Output: Updated parameters θ

- 1: **for** each minibatch $\mathcal{B} \subset \mathcal{D}$ **do**
- 2: **for** each $(x, a) \in \mathcal{B}$ **do**
- 3: $\tilde{r} \leftarrow \mathcal{G}(x)$ \triangleright harmless, general, variable length, may include placeholders
- 4: $y \leftarrow [\langle\text{think}\rangle, \tilde{r}, \langle/\text{think}\rangle, a]$
- 5: Tokenize $y \mapsto (y_1, \dots, y_T)$
- 6: Build mask $m_{1:T}$ where $m_t = 0$ for tokens in \tilde{r} and $m_t = 1$ for tokens in a \triangleright optionally include delimiter tokens
- 7: **end for**
- 8: $\mathcal{L} \leftarrow -\sum_{(x,a) \in \mathcal{B}} \sum_{t=1}^T m_t \log p_\theta(y_t | x, y_{<t})$
- 9: $\theta \leftarrow \theta - \eta \nabla_\theta \mathcal{L}$
- 10: **end for**

Since the teacher forces conditions on the entire prefix $y_{<t}$, the model can attend to \tilde{r} as privileged context during optimization, while gradients are applied only to the answer prediction. This reduces incentives to overfit to short answer templates and preserves expressive capacity, because the model is not penalized for mismatching the teacher-generated reasoning text.

Usage at inference. At inference time, decoding can either (i) omit the think region by prompting for answers only, or (ii) allow a think delimited region for internal deliberation, depending on the evaluation protocol. The core training mechanism remains the same, namely, reasoning tokens are never used as direct supervision targets.

Why Masked Reasoning Augmentation Preserves Reasoning Ability. We justify that masked reasoning augmentation (Sec. C.4) is a rational and effective surrogate for missing chain-of-thought (CoT) supervision: it avoids the degeneracy induced by short-answer-only tuning while not forcing imitation of teacher rationales, thereby preserving latent deliberation capacity.

Setup. Let p_0 denote the pre-trained (or instruction-tuned) initialization and p_θ the fine-tuned model. For each example $(x, a) \sim \mathcal{D}$, construct $y = [r, a]$ where $r = \langle\text{think}\rangle \tilde{r} \langle/\text{think}\rangle$ and a is the gold answer (Eq. 25). Let A be the set of answer-token positions, and R the set of reasoning-token positions in the tokenization $y_{1:T}$. The training loss is the masked NLL (Eq. 27)

$$\mathcal{L}(\theta) = -\mathbb{E}_{(x,a)} \left[\sum_{t \in A} \log p_\theta(y_t | x, y_{<t}) \right], \quad (28)$$

(optionally adding delimiter tokens to A does not change the arguments below).

Claim 1 (Masked augmentation reduces template overfitting). Assume a decoder factorization $p_\theta(y | x) = \prod_{t=1}^T p_\theta(y_t | x, y_{<t})$. Consider the answer-only tuning objective without any reasoning prefix:

$$\mathcal{L}_{\text{ans-only}}(\theta) = -\mathbb{E}_{(x,a)} \left[\log p_\theta(a | x) \right], \quad (29)$$

where the model learns $p_\theta(a | x)$ under a short and highly repetitive target format. If the target answers share a narrow template family (e.g., “The answer is A”), then $\mathcal{L}_{\text{ans-only}}$ admits low-loss solutions that allocate probability mass to a small set of high-frequency surface forms, yielding a biased decoder that collapses stylistic and intermediate-generation degrees of freedom.

Under masked augmentation, the supervised tokens $t \in A$ are predicted conditioned on a longer, variable prefix r :

$$p_\theta(a | x, r) = \prod_{t \in A} p_\theta(y_t | x, y_{<t}), \quad y_{<t} \supseteq r. \quad (30)$$

Since r is variable-length and lexically diverse, the conditional context distribution seen during training has higher entropy than in Eq. 29. This breaks the spurious shortcut of mapping $x \mapsto$ a fixed answer template independent of preceding

generation state, because the answer head must remain stable across a family of diverse prefixes. Operationally, the model is optimized to output the same a across many distinct r -contexts, which regularizes against brittle template memorization and maintains flexibility in generation dynamics before the answer.

Claim 2 (No-imitation property: the method does not teach or enforce teacher CoT). By construction, the mask sets $m_t = 0$ for all $t \in R$ (Eq. 26), hence the gradient decomposes as

$$\nabla_{\theta} \mathcal{L}(\theta) = -\mathbb{E}_{(x,a)} \left[\sum_{t \in A} \nabla_{\theta} \log p_{\theta}(y_t | x, y_{<t}) \right], \quad \frac{\partial \mathcal{L}}{\partial \log p_{\theta}(y_t | \cdot)} = 0 \quad \forall t \in R. \quad (31)$$

Therefore, masked augmentation cannot directly push p_{θ} to reproduce \tilde{r} or match the teacher’s reasoning distribution; it only uses \tilde{r} as conditioning noise/augmentation for predicting a . This avoids two common failure modes of distillation-style CoT training: (i) copying teacher-specific artifacts and (ii) penalizing valid alternative reasoning trajectories.

Claim 3 (Latent-deliberation preservation via prefix invariance). Define the desired robustness property: for a given instruction x , correct answering should be invariant to benign internal deliberation text r that does not leak the label. Formally, for a distribution $\mathcal{R}(x)$ over harmless reasoning prefixes, we want

$$p_{\theta}(a | x, r) \approx p_{\theta}(a | x, r'), \quad r, r' \sim \mathcal{R}(x), \quad (32)$$

while still allowing r to carry computational substrate during generation. Masked augmentation is exactly empirical risk minimization over random r -contexts:

$$\min_{\theta} \mathbb{E}_{(x,a)} \mathbb{E}_{r \sim \mathcal{R}(x)} \left[-\log p_{\theta}(a | x, r) \right]. \quad (33)$$

Optimizing Eq. 33 encourages p_{θ} to be stable under variations of the pre-answer hidden-state trajectory induced by diverse prefixes. Intuitively, the model is trained to remain competent after spending tokens in a think region, rather than being trained to emit the answer immediately. This directly targets the failure case of answer-only tuning, where decoding before the answer becomes a low-utility region and the model learns to shortcut.

Claim 4 (Connection to dropout-style regularization over prefixes). Masked augmentation can be viewed as a structured data augmentation on the conditioning context: r is a sampled perturbation of the prefix distribution that leaves the label a unchanged. As in classic augmentation, the supervised signal forces the predictor to rely on task-relevant information (the instruction x and structural tokens) rather than fragile surface regularities of a fixed answer template. Unlike standard dropout, this perturbation operates at the sequence level and explicitly exercises the model’s long-context attention and state evolution before producing a .

Practical implication. Claims 1–4 imply the method is rational under missing-CoT conditions: it (i) prevents collapse to short answer templates by training under diverse pre-answer prefixes, (ii) preserves freedom of internal reasoning because no gradients are applied to \tilde{r} , and (iii) encourages answer stability after variable-length latent deliberation, which is the minimal property needed to maintain reasoning-like behavior when explicit reasoning corpora are unavailable.

D. Experiment Details

D.1. Datasets and Benchmarks

Mol-Instructions (molecule and protein) (Fang et al., 2023). Mol-Instructions constructs instruction tuning data by aggregating licensed biomolecular sources and converting them into a unified instruction format, with additional task description diversification via human-written seeds expanded by an LLM and then manually reviewed, followed by explicit quality control to ensure reliability. It is organized into **three components**: molecule-oriented instructions covering molecular captioning, reactions, and design with 148.4K instructions across six tasks, protein-oriented instructions spanning five task categories for structure, function, activity, and design with 505K instructions, and biomolecular text instructions for information extraction and QA style NLP tasks with 53K instructions.

DNA-Chat (de Almeida et al., 2025). ChatNT converts existing DNA sequence benchmarks into instruction data by curating many English question answer templates per task and sampling a template per input sequence. For the Nucleotide

Transformer benchmark, it converts 18 binary or multilabel classification datasets into diverse instructions while keeping the original train-test splits. Data correctness and evaluation consistency are supported by retaining original dataset splits, using different questions in train versus test to probe English generalization, and reporting each task metric as defined in the corresponding benchmark, typically on up to 5,000 sampled test instances per task. The resulting instructions corpus is large, reported as 605M DNA tokens and 273M English tokens, and model training over the 27 task set is described as 7.8M samples over 2B tokens.

RNA-QA (Xiao et al., 2024b). RNA-QA is constructed from RNACentral (Bateman et al., 2011) by filtering RNAs with associated literature and then scraping and summarizing relevant papers to produce per RNA annotations, with a divide and conquer summarization pipeline that applies topic modeling to group papers and then summarizes each group before a final aggregation summary. The paper reports an initial filter of roughly 420,000 literature-linked RNAs, refined to 407,616 RNAs, with sequences truncated or filtered to a length of at most 1024 nucleotides to fit the sequence encoder input limit, and each RNA is paired with an abstract style description. For instruction tuning, the dataset decomposes these annotations into more targeted QA pairs using an LLM, producing multiple QA pairs per RNA and explicitly noting 5 to 14 QA pairs per RNA in the collection pipeline description.

GEO-AT. GEO-AT is a unified all-atom instruction dataset constructed for connector alignment and structure conditioned LLM adaptation under end-to-end finetuning, prioritizing compactness and high supervision density. It aggregates three modalities: (i) molecules, using 10K chemical to text captioning pairs from Mol-Llama-Instruct (Kim et al., 2025); (ii) proteins, using 10K high confidence UniProt (Consortium, 2019) entries (annotation score 5/5) with verified PDB (Burley et al., 2017) 3D structures, excluding multi conformer sequences to preserve unambiguous structural supervision; and (iii) nucleic acids, using 10K instruction following samples from ChatNT (5K DNA, 5K RNA) (de Almeida et al., 2025). For instances lacking experimentally resolved 3D structures, geometries are generated via the pipeline in App. C.2. Each modality reserves 200 held-out test samples, with the remaining examples used for training. All the baselines for this benchmark are tuned on this dataset. Table 12 summarizes data sources and counts across training stages and modalities.

D.2. Baselines

Baselines include general instruction-tuned LLMs, domain-adapted chemistry and biomolecule LLMs, and explicit reasoning variants. General chat and backbone references include Alpaca (Taori et al., 2023), Baize (Xu et al., 2023a), ChatGLM (GLM et al., 2024), LLaMA-2 (Touvron et al., 2023), Vicuna-v1.5 (Zheng et al., 2023), Qwen2.5 (Bai et al., 2025), Llama-3 (Grattafiori et al., 2024), Mistral-3 (Liu et al., 2026), GLM-4-9B (GLM et al., 2024), and Qwen3-8B (Yang et al., 2025a), providing broad instruction-following capacity without structural specialization. Science and chemistry-oriented baselines include Galactica-6.7B (Taylor et al., 2022), Text+Chem T5 (Christofidellis et al., 2023), and Molt5 (Pei et al., 2024), which incorporate scientific or molecular pretraining objectives to improve chemistry-text alignment. Biomolecular instruction baselines include Mol-Instructions (Fang et al., 2023), which fine-tune Llama backbones on Mol-Instructions datasets, and Mol-LLama (Kim et al., 2025), which further targets molecule-centric alignment. Reasoning-focused general baselines include DeepSeek-R1-D-Qwen-7B (Guo et al., 2025a) and Mistral-3-8B-Reasoning (Liu et al., 2026), used to assess gains attributable to explicit reasoning post-training rather than modality grounding. For protein-specific models, ProtLLM (Zhuo et al., 2024), ProteinGPT (Xiao et al., 2024a), and ProtChatGPT (Wang et al., 2024) are selected.

Rationale of Selection. Baselines are selected to isolate gains from structure grounding under realistic compute and model-size constraints. General LLMs are restricted to recent, open-source instruction-tuned backbones, covering both reasoning and non-reasoning variants, with parameters largely aligned to the 6–8B regime to match the available training and evaluation budget. Modality-specific baselines prioritize strong, recent domain models that natively accept molecular or biomolecular structural inputs or molecule-aware tokenizations, and that report competitive performance on closely related instruction or QA benchmarks, enabling a fair comparison between sequence-only adaptation and explicit structure-conditioned modeling.

D.3. Benchmark Metrics

Text generation quality. For free-form descriptions and open-ended instruction responses, we report n-gram overlap, sequence-level recall, and semantic matching metrics. **BLEU-2/4** (\uparrow) quantify modified n-gram precision with a brevity penalty. **ROUGE-1/2/L** (\uparrow) measure unigram/bigram overlap and longest-common-subsequence (LCS) similarity, capturing content coverage and ordering robustness. **METEOR** (\uparrow) emphasizes alignment with stemming/synonymy and includes a fragmentation penalty, improving sensitivity to paraphrases. For embedding-level semantic similarity, we report **BERTScore**

(\uparrow), computed via token embedding cosine matches between hypothesis and reference:

$$\text{BERTScore}(y, \hat{y}) = \frac{1}{|y|} \sum_{t \in y} \max_{s \in \hat{y}} \cos(\mathbf{e}_t, \mathbf{e}_s), \quad (34)$$

with precision/recall/F1 variants reported per benchmark convention. We use these metrics when multiple valid phrasings exist and surface overlap and semantic faithfulness jointly.

Regression error. For scalar property prediction, we use **MAE** (\downarrow), the mean absolute error:

$$\text{MAE} = \frac{1}{N} \sum_{i=1}^N |\hat{z}_i - z_i|, \quad (35)$$

where z_i and \hat{z}_i denote the ground-truth and predicted targets.

Classification. For DNA tasks with class imbalance, we report **Matthews correlation coefficient (MCC)** (\uparrow), which correlates predictions and labels and remains informative under skewed marginals:

$$\text{MCC} = \frac{TP \cdot TN - FP \cdot FN}{\sqrt{(TP + FP)(TP + FN)(TN + FP)(TN + FN)}}. \quad (36)$$

Exact-match and edit distance. For structured-string outputs (e.g., canonical answers or sequence-like targets), we report **Exact** (\uparrow) accuracy and character-level **Levenshtein** distance (\downarrow):

$$\text{Exact} = \mathbb{1}[\hat{y} = y], \quad \text{Lev}(y, \hat{y}) = \min_{\pi \in \mathcal{E}(y \rightarrow \hat{y})} |\pi|, \quad (37)$$

where \mathcal{E} denotes the set of edit sequences (insert/delete/substitute) transforming y into \hat{y} .

Molecule validity and similarity (structure-aware). For molecule generation, we evaluate both chemical validity and structure similarity. **Validity** (\uparrow) is the fraction of outputs parsable into valid molecules (e.g., via RDKit). To quantify similarity between generated and reference molecules, we compute fingerprint Tanimoto similarity (FTS, \uparrow) using multiple representations, including **RDKit** fingerprints, **MACCS** keys, and **Morgan** fingerprints:

$$\text{FTS}(m, \hat{m}) = \text{Tan}(\phi(m), \phi(\hat{m})) = \frac{\langle \phi(m), \phi(\hat{m}) \rangle}{\|\phi(m)\|_1 + \|\phi(\hat{m})\|_1 - \langle \phi(m), \phi(\hat{m}) \rangle}, \quad (38)$$

where $\phi(\cdot) \in \{0, 1\}^d$ is a binary fingerprint and Tan denotes Tanimoto similarity. We additionally report **BLEU** (\uparrow) and **Levenshtein** (\downarrow) for string-level similarity when the target is provided as a SMILES-like representation, but prioritize validity and fingerprint similarity to reflect chemically meaningful agreement.

D.4. Detailed Benchmark Results

This section reports the full Mol-Instructions (Fang et al., 2023) benchmark results. The main paper Tab. 3 is restricted to at most two metrics per task for layout compactness, whereas the appendix exposes the complete metric suite. Across tasks, Cuttlefish attains top rank on essentially all reported metrics, indicating consistent gains rather than metric-specific overfitting.

Molecular description and property (Tab. 13). Cuttlefish achieves best performance across the lexical overlap metrics for molecular captioning and simultaneously yields the lowest error on property regression, indicating joint improvements in structure-conditioned text and property grounding. The only non-leading captioning metric is a mid-order ROUGE variant, where Cuttlefish remains competitive.

Description-guided molecule design (Tab. 14). Cuttlefish dominates generation quality and edit-distance metrics, and also leads across multiple fingerprint similarity measures, suggesting improved alignment between instruction semantics and generated molecular structure. Validity is saturated at the top tier, indicating that gains are driven by chemical plausibility

Table 13. Detailed results on molecular captioning and property prediction tasks from the Mol-Instruction benchmark. Official splits are used for testing Cuttlefish, Qwen, and Mol-Llama models; others are taken from the benchmark leaderboard.

Model	Molecular Description						Property MAE \downarrow
	BLEU-2 \uparrow	BLEU-4 \uparrow	ROUGE-1 \uparrow	ROUGE-2 \uparrow	ROUGE-L \uparrow	METEOR \uparrow	
Alpaca-7B	0.068	0.014	0.178	0.041	0.136	0.107	322.109
Baize-7B	0.064	0.015	0.189	0.053	0.148	0.106	261.343
LLaMA-2-7B	0.059	0.014	0.164	0.066	0.148	0.184	5.553
Vicuna-v1.5-13B	0.052	0.011	0.151	0.055	0.130	0.168	860.051
Galactica-6.7B	0.024	0.008	0.074	0.015	0.063	0.065	0.568
Qwen2.5-7B	0.435	0.356	0.581	0.491	0.572	0.538	0.182
Mol-Ins.-Llama-2-7B	0.217	0.143	0.337	0.196	0.291	0.291	0.013
Mol-Ins.-Llama-3.1-8.3B	0.419	0.361	0.719	0.646	0.709	0.637	15.059
Mol-LLaMA-2-7B	0.478	0.425	0.761	0.698	0.750	0.701	0.0035
Mol-LLaMA-3.1-8.3B	0.476	0.426	0.767	0.708	0.759	0.707	0.0039
Cuttlefish-8.3B	0.481	0.442	0.785	0.681	0.766	0.715	0.0030

Table 14. Detailed results on the description-guided molecule design task from the Mol-Instructions benchmark. Official splits are used for testing Cuttlefish, Qwen, and Mol-LLaMA models; other baselines are taken from the benchmark leaderboard.

Model	Exact \uparrow	BLEU \uparrow	Levenshtein \downarrow	RDKit FTS \uparrow	MACC FTS \uparrow	Morgan FTS \uparrow	Validity \uparrow
Alpaca-7B	0.000	0.004	51.088	0.006	0.029	0.000	0.002
Baize-7B	0.000	0.006	53.796	0.000	0.000	0.000	0.002
ChatGLM-6B	0.000	0.004	53.157	0.005	0.000	0.000	0.005
LLaMA-2-7B	0.000	0.003	59.864	0.005	0.000	0.000	0.003
Vicuna-v1.5-13B	0.000	0.006	60.356	0.006	0.001	0.000	0.001
Galactica-6.7B	0.000	0.192	44.152	0.135	0.238	0.088	0.992
Text+Chem T5	0.097	0.508	41.819	0.352	0.474	0.353	0.721
MolT5	0.112	0.546	38.276	0.400	0.538	0.295	0.773
Mol-Ins.-Llama-2-7B	0.002	0.345	41.367	0.231	0.412	0.147	1.000
Mol-Ins.-Llama-3.1	0.025	0.521	38.742	0.358	0.520	0.221	1.000
Mol-LLaMA-3.1-8.3B	0.012	0.638	18.917	0.392	0.534	0.220	0.876
Qwen2.5-7B	0.001	0.434	306.144	0.207	0.348	0.121	0.772
Cuttlefish-8.3B	0.019	0.668	16.029	0.422	0.583	0.287	1.000

Table 15. Detailed results on the forward reaction prediction task from the Mol-Instructions benchmark. Official splits are used for testing Cuttlefish, Qwen, and Mol-LLaMA models; other baselines are taken from the benchmark leaderboard.

Model	Exact \uparrow	BLEU \uparrow	Levenshtein \downarrow	RDKit FTS \uparrow	MACC FTS \uparrow	Morgan FTS \uparrow	Validity \uparrow
Alpaca-7B	0.000	0.065	41.989	0.004	0.024	0.008	0.138
Baize-7B	0.000	0.044	41.500	0.004	0.025	0.009	0.097
ChatGLM-6B	0.000	0.183	40.008	0.050	0.100	0.044	0.108
LLaMA-2-7B	0.000	0.020	42.002	0.001	0.002	0.001	0.039
Vicuna-v1.5-13B	0.000	0.057	41.690	0.007	0.016	0.006	0.059
Galactica-6.7B	0.000	0.468	35.021	0.156	0.257	0.097	0.946
Text+Chem T5	0.239	0.782	20.413	0.705	0.789	0.652	0.762
Mol-Ins.-Llama-2-7B	0.045	0.654	27.262	0.313	0.509	0.262	1.000
Mol-Ins.-Llama-3.1	0.503	0.883	13.410	0.756	0.863	0.708	1.000
Mol-LLaMA-3.1-8.3B	0.440	0.912	17.120	0.724	0.859	0.665	1.000
Qwen2.5-7B	0.000	0.542	140.000	0.163	0.240	0.090	0.953
Cuttlefish-8.3B	0.551	0.964	19.280	0.792	0.879	0.722	1.000

and target matching rather than trivial validity filtering. The only top-2 outcome occurs on one fingerprint similarity, plausibly reflecting descriptor-specific bias toward particular scaffold statistics.

Forward reaction prediction (Tab. 15). Cuttlefish attains the best exact match and overall generation quality, while also leading on structure-based similarity and maintaining perfect validity, supporting improved mechanistic consistency in

Table 16. Detailed results on the reagent prediction task from the Mol-Instructions benchmark. Official splits are used for testing Cuttlefish, Qwen, and Mol-LLaMA models; other baselines are taken from the benchmark leaderboard.

Model	Exact↑	BLEU↑	Levenshtein↓	RDKit FTS↑	MACC FTS↑	Morgan FTS↑	Validity↑
Alpaca-7B	0.000	0.026	29.037	0.029	0.016	0.001	0.186
Baize-7B	0.000	0.051	30.628	0.022	0.018	0.004	0.099
ChatGLM-6B	0.000	0.019	29.169	0.017	0.006	0.002	0.074
LLaMA-2-7B	0.000	0.003	28.040	0.037	0.001	0.001	0.001
Vicuna-v1.5-13B	0.000	0.010	27.948	0.038	0.002	0.001	0.007
Galactica-6.7B	0.000	0.141	30.760	0.036	0.127	0.051	0.995
Text+Chem T5	0.000	0.225	49.323	0.039	0.186	0.052	0.313
Mol-Ins.-Llama-2-7B	0.044	0.224	23.167	0.237	0.364	0.213	1.000
Mol-Ins.-Llama-3.1	0.101	0.648	18.326	0.412	0.521	0.375	1.000
Mol-LLaMA-3.1-8.3B	0.132	0.495	49.230	0.411	0.521	0.361	1.000
Qwen2.5-7B	0.039	0.428	64.420	0.258	0.378	0.257	0.955
Cuttlefish-8.3B	0.149	0.640	46.991	0.509	0.549	0.450	1.000

Table 17. Detailed results on the retrosynthesis task from the Mol-Instructions benchmark. Official splits are used for testing Cuttlefish, Qwen, and Mol-LLaMA models; other baselines are taken from the benchmark leaderboard.

Model	Exact↑	BLEU↑	Levenshtein↓	RDKit FTS↑	MACC FTS↑	Morgan FTS↑	Validity↑
Alpaca-7B	0.000	0.063	46.915	0.005	0.023	0.007	0.160
Baize-7B	0.000	0.095	44.714	0.025	0.050	0.023	0.112
ChatGLM-6B	0.000	0.117	48.365	0.056	0.075	0.043	0.046
LLaMA-2-7B	0.000	0.036	46.844	0.018	0.029	0.017	0.010
Vicuna-v1.5-13B	0.000	0.057	46.877	0.025	0.030	0.021	0.017
Galactica-6.7B	0.000	0.452	34.940	0.167	0.274	0.134	0.984
Text+Chem T5	0.141	0.765	24.043	0.685	0.765	0.585	0.698
Mol-Ins.-Llama-2-7B	0.009	0.705	31.227	0.283	0.487	0.230	1.000
Mol-Ins.-Llama-3.1	0.333	0.842	17.642	0.704	0.815	0.646	1.000
Mol-LLaMA-3.1-8.3B	0.340	0.877	38.324	0.708	0.822	0.601	1.000
Qwen2.5-7B	0.000	0.579	144.000	0.168	0.291	0.112	0.939
Cuttlefish-8.3B	0.395	0.854	26.310	0.747	0.839	0.681	1.000

reaction outcome generation.

Reagent prediction (Tab. 16). Cuttlefish ranks top-1 on exact match and all structure-based similarity metrics while maintaining perfect validity, indicating superior condition inference and chemically consistent reagent set generation. A single text-overlap metric is top-2, consistent with synonymy and ordering non-identifiability in reagent lists that weakly correlate with correctness under n-gram scoring.

Retrosynthesis (Tab. 17). Cuttlefish achieves the best exact match and fingerprint similarities with saturated validity, suggesting improved decomposition of target products into plausible precursors rather than purely string-level matching. BLEU is top-2, plausibly driven by multiple valid precursor sets and canonicalization variability that penalize lexical overlap despite chemically aligned outputs.

OpenQA (Tab. 18). This task is predominantly text-only, lacking a specific molecular input, so structure-conditioning advantages are expected to be attenuated. Nevertheless, Cuttlefish remains competitive on lexical overlap and achieves the strongest semantic similarity, indicating preserved general instruction-following and paraphrase robustness under multimodal training. This pattern suggests that structure alignment acts as a complementary inductive bias that improves biomolecular semantics without sacrificing text-only competence.

D.5. Completion and Reasoning Cases

Examples of Reasoning. Figs. 8 – 12 present qualitative reasoning examples across molecule, protein, DNA, and RNA tasks, illustrating how Cuttlefish integrates all-atom structural evidence into intermediate reasoning. In molecular captioning and molecular QA (Figs. 8 and Fig. 9), the model explicitly conditions its predictions on geometric and physicochemical

Table 18. Detailed results on the OpenQA task from the Mol-Instructions benchmark. Official splits are used for testing Cuttlefish, Qwen, and Mol-LLaMA models; other baselines are taken from the benchmark leaderboard.

Model	BLEU↑	ROUGE-1↑	BertScore↑
Alpaca-7B	0.003	0.088	0.824
Baize-7B	0.005	0.100	0.811
ChatGLM-6B	0.003	0.090	0.795
LLaMA-2-7B	0.003	0.100	0.814
Vicuna-v1.5-13B	0.004	0.097	0.814
Galactica-6.7B	0.000	0.039	0.794
PMC_LLaMA	0.007	0.788	0.625
Mol-Ins.-LLama-2-7B	0.024	0.221	0.837
Mol-Ins.-LLama-3.1	0.010	0.198	0.846
Mol-LLaMA-3.1-8.3B	0.024	0.134	0.812
Qwen2.5-7B	0.793	0.204	0.846
Cuttlefish-8.3B	0.117	0.342	0.884

Sequence C=C/C1=CC2=C(C=C1)OC(=C2C)C3=CC=C(C=C3)OC4=C(C=CC(=C4)C5=C(C6=C(O5)C=CC(=C6)/C=C/C)C)O

System You are a structure grounded chemistry assistant. You must reason before answering.
Requirements:
1. First produce `<think>` with a brief, substantive rationale grounded in the provided context and the molecular representation.
2. Then produce `<answer>` containing the assistant response sentence.
3. Then output a final line: Final answer: ..., where the text matches `<answer>` exactly.
4. Do not add any extra text outside these three outputs.
Format strictly:
`<think>...</think>`
`<answer>...</answer>`
Final answer: ..."

Instruction Could you provide a description of this molecule?
Molecule <mol>.

Response `<think>`The user asks for a description, but the provided context already supplies the key factual descriptor.
To avoid hallucinating functional or class annotations not supported by the dialogue, I will restate the provenance claim succinctly.
I will keep the answer to a single sentence aligned with the given assistant cue.`</think>`
`<answer>`The molecule is a natural product found in Piper aequale with data available.`</answer>`
Final answer: The molecule is a natural product found in Piper aequale with data available."

Ground Truth The molecule is a natural product found in Piper aequale with data available ...

Figure 8. Reasoning example on the molecular captioning task. The model accepts a molecular input (along with its structure) and the instructions. The output will contain the reasoning part for the question.

cues (such as steric bulk, ionization state, and functional group-driven permeability) rather than relying on sequence-level correlations. This behavior reflects the effect of Geometry Grounding Adapter, which exposes verifiable geometric information to the LLM.

For macromolecular modalities, Cuttlefish exhibits domain-aware and task-specific reasoning grounded in structure. In protein captioning (Fig. 10), functional conclusions are tied to structurally localized domains and interaction partners, avoiding unsupported mechanistic extrapolation. Similarly, in DNA and RNA (Figs. 11 and Fig. 12), the model produces conservative, evidence-aligned judgments (e.g., promoter presence) without hallucinating precise motif locations or regulatory mechanisms. These examples indicate that geometry-grounded tokens encourage faithful abstraction, thereby preventing hallucinations.

Across all cases, the reasoning traces also demonstrate the scalability benefits of Scaling-Aware Patching. Complex all-atom inputs are selectively summarized through instruction-conditioned patching, enabling the model to retain structurally salient regions while suppressing redundant context. As a result, Cuttlefish maintains coherent reasoning across heterogeneous sequence lengths and structural complexities, supporting its effectiveness as a unified structure-aware LLM.

Entity type recognition. Fig. 13 illustrates representative structure-only prompts demonstrating that the model reliably infers entity type without any auxiliary textual cues. Given only structural inputs, Cuttlefish correctly classifies the underlying entity as a small molecule, protein, DNA, or RNA. Notably, DNA and RNA are disambiguated solely from structural signals, without explicit sequence information. These examples validate that the model learns modality-specific structural priors and can perform accurate entity-type recognition from structure alone, establishing a prerequisite for downstream

Sequence CO[C@]12CC[C@@]3(C[C@@H]1[C@](C)(O)C(C)(C)C)[C@H]1Cc4cc(O)c5c4[C@@]3(CCN1CC1CC1)[C@H]2O5

System You are a chemistry research assistant, and I'd like to test your professional ability on molecule understanding, please complete the following task:
 You are provided with a molecule and asked a question about the molecule's property-related knowledge (property means physical, biological or chemical property in various environments or reactions), with four options given. Three of these options do not describe the given molecule, and you must select the correct option.
 Notice that here are some rules you need to follow:
 1. Your answer for each question should be one of A/B/C/D, which corresponds to the four options.
 2. Please give me your ANSWER for the given instances in the format 'Answer: ...'

Instruction Molecule: <mol>
 Question: What is the right information about this molecule's absorption?
 - Option A: It undergoes very little absorption following oral or topical administration.
 - Option B: It has poor gastrointestinal absorption and is therefore formulated as a sublingual tablet.
 - Option C: It has minimal oral absorption and its use has not been linked to instances of acute liver injury.
 - Option D: It has good absorption and enhanced oral bioavailability.

Response <think>The structure is a **bulky, rigid polycyclic scaffold with multiple fused rings**, which tends to reduce passive diffusion through the gastrointestinal epithelium. It includes a **tertiary amine**, so it will be protonated at physiological pH, increasing aqueous solubility but decreasing membrane permeability for oral uptake. It also **contains phenolic and ether oxygens**, adding polarity and hydrogen bonding capacity, further penalizing gut permeability. A common mitigation for poor gastrointestinal absorption of ionizable, permeability limited compounds is non GI delivery such as sublingual administration. Therefore the option stating poor gastrointestinal absorption with sublingual formulation is most consistent.</think>
 <answer>B</answer>
Final answer: B

Ground Truth Answer: B

Figure 9. Reasoning example on the molecular QA task. The model accepts a molecular input (along with its structure) and the instructions. The output will contain the reasoning part for the question.

structure-grounded reasoning.

Structure ensures faithful reasoning. Fig. 14 illustrates a reliability gap driven by structural grounding. Cuttlefish extracts salient structure-conditioned cues and produces a coherent property-level rationale aligned with the correct absorption choice, whereas the Q-Former variant overgeneralizes from superficial motifs and thus selects an incorrect option, reflecting connector-bottleneck-induced distortion or hallucination. The sequence-only variant cannot access fine-grained structural evidence, leading to low-confidence reasoning that guesses the answer but lacks a verifiable structure-based justification, highlighting the importance of detailed structure for faithful inference.

D.6. Data Contamination Analysis

Table 19 quantifies potential train–test contamination between Mol-Instructions (Fang et al., 2023) and the training corpus of GEO-AT using both entity-level overlap and an n-gram lexical criterion. Concretely, for each benchmark task with test set $\mathcal{D} * \text{test}$ and GEO-AT training set $\mathcal{D} * \text{train}$, we measure the 13-gram overlap rate as

$$\text{OR}_{13} = \frac{1}{|\mathcal{D} * \text{test}|} \sum_{x \in \mathcal{D} * \text{test}} \mathbb{1}!(\mathcal{G} * 13(x) \cap \mathcal{G} * 13(\mathcal{D} * \text{train}) \neq \emptyset), \quad (39)$$

where $\mathcal{G} * 13(x)$ denotes the set of contiguous 13-token substrings (13-grams) extracted from the text fields of example x (e.g., instruction, input prompt, and/or target text, following the benchmark format), and $\mathcal{G} * 13(\mathcal{D} * \text{train}) = \bigcup_{x' \in \mathcal{D} * \text{train}} \mathcal{G} * 13(x')$ (Brown et al., 2020). We adopt 13-grams because exact long-span matches are unlikely to occur by chance, making OR_{13} a conservative indicator of near-duplicate textual leakage beyond exact entity identity. Entity-level overlap complements this by detecting cases where the same underlying biological or chemical entity appears in both training and test splits.

Overall, the overlap remains low across tasks in Tab. 19. Protein-oriented tasks show relatively higher entity-level overlap, which is expected since both GEO-AT and several Mol-Instructions datasets source proteins from UniProt (Consortium, 2019). To ensure a fair comparison, we perform explicit decontamination: before fine-tuning, we remove from $\mathcal{D}_{\text{train}}$ any example that overlaps with a benchmark test instance under either criterion (entity match or 13-gram match). This uniform filtering ensures that reported performance reflects generalization rather than memorization or benchmark leakage.

Sequence MAQSGGDQRAVGVADPEESSPNMIVYCKIEDIITKMQDDKTGGVPIRTVKSFLSKIPSVTGTDIVQWLMKNLSIEDPVEAIHL GSLIAAQGYIFPISDHVLTMKDDGTFYRFQAPYFWPSNCWEPENTDYAIYLCKRTMQNKARLEADYEAENLARLQRAFARKWEFIFMQ AEAQVKIDRKDKDTERKILDSQERAFFWDVHRPVPGCVNTTEMDIRKCRRLKNPQKVKKSVYGVTEESQAQSPVHVLSPQIRKTTKEDIR KQITFLNAQIDRHCLKMSKVAESLIAYTEQYVEYDPLITPAEPSNPWISDDVALWDIEMSKEPSQQRVKRWGFSFDEILKDQVGRDQFLRF LESEFSSENLRFWLAVQDLKKQPLQDVAKRVEEIWQEFLAPGAPSAINLDHSYEITSQNVKDGGRYTFEDAQEHIYKLMKSDSYARFLR SNAYQDLLLAKKKGKSLAGKRLTGLMQSS,

System You are a helpful assistant specializing in protein analysis and biology. The instruction that describes a task is given, paired with protein structure. Write a response that appropriately completes the request."

Instruction Could you provide a detailed description of the protein structure <STRUCTURE> and its function?"

Response <think>The request asks for structure and function, and the provided completion specifies the functional mechanism, the responsible domain, and interaction partners that modulate activity and localization.\nI will restate these points with equivalent wording, avoid adding unsupported structural claims, and retain the experimental recommendations and isoform caveat.</think>\n<answer>This protein negatively regulates **GPCR signaling by functioning as a GAP for G α subunits**. By accelerating the intrinsic GTP hydrolysis of G α , it promotes the inactive GDP bound state and suppresses downstream signal propagation. The key structural determinant is the central RGS domain, which binds G α with high affinity and catalytically enhances G α mediated GTP hydrolysis.\n\nA major functional assembly is a heterodimer with the atypical G β 5 subunit (GNB5), where the RGS6–GNB5 complex increases GNAO1 GTPase activity. Additional reported partners include GNAI1 and RGS7BP, with RGS7BP influencing subcellular distribution of the RGS–GNB5 complex. Association with GNB5 supports nuclear translocation, so GNB5 and RGS7BP are important determinants of both localization and effective GAP activity.\n\nMultiple isoforms may exist, and isoform variation can alter interaction specificity, targeting, and catalytic potency. Functional characterization should therefore quantify G α GTP hydrolysis with and without GNB5 and RGS7BP and control for isoform dependent effects.</answer>

Ground Truth Answer: This protein functions as a regulator of **G protein-coupled receptor (GPCR) signaling by acting as a GTPase-accelerating protein (GAP) for G α subunits**. It inhibits signal transduction by increasing the intrinsic GTPase activity of G α proteins, thereby driving them into their inactive, GDP-bound state. The central RGS domain mediates high-affinity interaction with G α and is responsible for accelerating G α -catalyzed GTP hydrolysis.\n\nFunctionally relevant interactions include formation of a heterodimer with the atypical beta subunit G β 5 (GNB5); the RGS6–GNB5 dimer specifically enhances GNAO1 GTPase activity. The protein also interacts with GNAI1 and with RGS7BP, the latter interaction modulating the subcellular disposition of the RGS–GNB5 heterodimer. Binding to GNB5 promotes translocation of the complex to the nucleus, so consider GNB5 and RGS7BP as key determinants of both activity and localization.\n\nBe aware that additional isoforms of this protein appear to exist; isoform diversity may influence interaction profiles, subcellular targeting, and GAP activity. When investigating its function, assay G α GTP hydrolysis in the presence and absence of GNB5 and RGS7BP and account for possible isoform-specific effects."

Figure 10. Reasoning example on the GEO-AT protein captioning task. The model accepts a protein and its structure, and the instructions as input. The output will contain the reasoning part before the final captioning answer.

D.7. Training Efficiency Analysis

Figure 15 (a–d) characterizes how Cuttlefish improves scalability relative to sequence-centric baselines ChatNT (de Almeida et al., 2025) and RNA-GPT (Xiao et al., 2024b) as structural size and model scale increase. (a) shows that baseline structural token usage grows near-linearly with node count, reflecting weakly adaptive interfaces that directly expose expanding structures to the LLM context. In contrast, Cuttlefish maintains a substantially lower structural budget at large entities by activating Scaling-Aware Patching to select instruction-relevant anchors and grow to patches. (b) Further indicates that the structural-to-language token composition is acceptable as node count increases, with a clear controllable trend in the token usage ratio.

The remaining panels link token efficiency to practical computing. (c) decomposes GPU memory usage into EGNN encoder, fusion blocks, and the LLM, showing that memory growth is dominated by the LLM backbone, while the incremental cost of structure processing and fusion grows sublinearly with node count under Cuttlefish’s adaptive patching. This contrasts with baselines where increased structural tokens directly inflate LLM-side activation and attention costs. (d) reports training hours as a function of training token count for different backbone sizes (1B–13B), illustrating the superlinear time growth as tokens increase and highlighting why controlling structural tokenization is critical for feasible scaling. Together, (a–d) support that Geometry Grounding Adapter and Scaling-Aware Patching jointly decouple structural resolution from LLM context length, yielding more stable memory footprints and improved end-to-end training efficiency.

Sequence:

CO[C@]12CC[C@@]3(C[C@@H]1[C@](C)(O)C(C)(C)C)[C@H]1Cc4ccc(O)c5c4[C@@]3(CCNC1CC1)[C@H]2O5

System You are a chemistry research assistant, and I'd like to test your professional ability on molecule understanding, please complete the following task:
You are provided with a molecule and asked a question about the molecule's property-related knowledge (property means physical, biological or chemical property in various environments or reactions), with four options given. Three of these options do not describe the given molecule, and you must select the correct option.
Notice that here are some rules you need to follow:
1. Your answer for each question should be one of A/B/C/D, which corresponds to the four options.
2. Please give me your ANSWER for the given instances in the format 'Answer: ...'

Instruction Molecule: <mol>
Question: What is the right information about this molecule's absorption?
- Option A: It undergoes very little absorption following oral or topical administration.
- Option B: It has poor gastrointestinal absorption and is therefore formulated as a sublingual tablet.
- Option C: It has minimal oral absorption and its use has not been linked to instances of acute liver injury.
- Option D: It has good absorption and enhanced oral bioavailability.

Ground Truth Answer: B

Cuttlefish

Response <think> The molecule exhibits a large, rigid, polycyclic scaffold with substantial steric bulk and limited conformational flexibility. Although it contains several heteroatoms, the overall architecture remains highly lipophilic and sterically congested, which typically restricts passive diffusion across the gastrointestinal epithelium. Compounds with these characteristics often show poor oral absorption and are instead delivered through alternative routes to improve systemic exposure and avoid extensive first-pass metabolism. Such absorption behavior is consistent with formulations designed for sublingual administration rather than standard oral dosing.
</think> The correct answer is **Answer: B.** ✓

Q-Former variant

Response <think> The molecule contains multiple oxygen atoms and appears chemically complex, suggesting the presence of polar functional groups. Polar functionalities are commonly associated with enhanced solubility and improved interaction with biological membranes. Based on these features, the compound is expected to be readily absorbed following oral administration and to exhibit favorable bioavailability without requiring specialized formulation strategies.</think>

Answer: D ✗

Sequence-only variant

Response <think> The molecule appears relatively large and structurally complex, which may influence its absorption properties. However, without a detailed understanding of how its structural features interact with biological barriers, the absorption behavior remains uncertain.

Given that some large bioactive compounds are delivered using non-standard oral routes, a formulation that avoids conventional gastrointestinal absorption seems plausible. I am not fully certain; however, based on the available context, option B appears to be the most plausible.</think>

Answer: B ✓

Figure 14. Qualitative comparison of three Cuttlefish model variants on a molecular absorption multiple-choice question. The figure shows (top) the input small-molecule SMILES, the system prompt and instruction with four options, and the ground-truth label, and (bottom) the corresponding responses from Cuttlefish, a Q-Former variant, and a sequence-only variant, with highlighted text spans indicating the correctness of rationale cues.

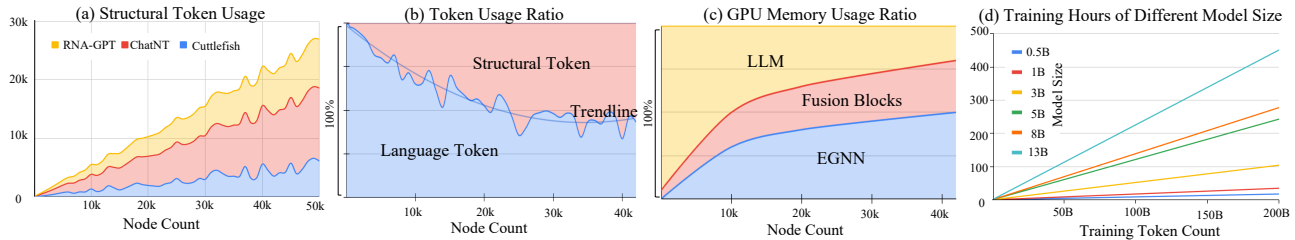


Figure 15. Training efficiency analysis of Cuttlefish versus ChatNT and RNA-GPT. (a) Structural token usage versus node count. (b) Structural token usage ratio (structural vs. language tokens) versus node count, with a fitted trendline. (c) GPU memory usage ratio decomposed into EGNN, fusion blocks, and LLM components as node count increases. (d) Training hours versus training token count for backbones from 0.5B to 13B parameters, with the y-axis regularized to H100-80G GPU hours (LoRA applied).

language capacity without saturating early. Gains are most pronounced from 0.5B to 3B, while improvements beyond 7B become incremental, suggesting diminishing returns once sufficient language expressivity is reached. Importantly, strong DNA and RNA performance at 7B–14B confirms that geometry-grounded tokens remain effective at scale rather than being overshadowed by larger text priors.

E.2. Effect of LLM Adaptation Epochs

Tab. 21 studies the number of epochs used in the LLM adaptation stage. Performance peaks at 2–3 epochs across modalities, while additional training leads to consistent degradation. This trend indicates that moderate adaptation is sufficient for

Table 19. Entity-level and 13-gram overlap rates across 3 types of tasks from benchmark Mol-Instructions (before filtered).

Dataset / Task	Entity-Level Overlap Rate	13-gram Overlap Rate
<i>Molecule-oriented tasks</i>		
Molecule description generation	5.57%	6.85%
Description-guided molecule design	0.78%	0.88%
Forward reaction prediction	5.02%	2.59%
Retrosynthesis	5.07%	2.61%
Reagent prediction	1.34%	0.71%
Property prediction	3.47%	2.21%
<i>Protein-oriented tasks</i>		
Protein design	5.68%	3.59%
Protein functional description	4.97%	3.20%
Catalytic activity prediction	5.58%	3.30%
Domain/motif prediction	1.81%	1.32%
Protein structural prediction	2.14%	1.79%
<i>Biomolecular text (NLP) tasks</i>		
True or False question	3.79%	1.95%
Multiple-choice question	2.86%	1.94%
Chemical entity recognition	1.61%	1.07%
Chemical-disease interaction extraction	2.74%	2.24%
Chemical-protein interaction extraction	2.96%	2.09%
Open question	3.66%	2.64%

Table 20. Ablation on different model sizes. Qwen-2.5 is used as the base model as it has the widest size coverage. Each variant is evaluated on GEO-AT with BERTScore reported.

Model Size	Molecule	Protein	DNA&RNA	Average
0.5B	0.453	0.422	0.382	0.419
1.5B	0.586	0.577	0.544	0.569
3B	0.608	0.578	0.621	0.602
7B	0.863	0.816	0.832	0.840
14B	0.897	0.861	0.834	0.864

Table 22. Ablation on four pooling methods (fine-designed weighted pooling, mean/max/min pooling), evaluated on GEO-AT.

Pooling	Molecule	Protein	DNA&RNA	Average	Avg. Drop
Weighted	0.875	0.896	0.816	0.862	0.00%
Mean	0.848	0.812	0.802	0.821	4.14%
Max	0.831	0.821	0.796	0.816	4.60%
Min	0.851	0.777	0.786	0.804	5.76%

aligning the frozen LLM with structure-grounded tokens, whereas over-training induces overfitting and harms generalization. These results motivate the use of early stopping in the adaptation phase and validate the efficiency of Geometry Grounding Adapter in rapidly injecting geometric information.

E.3. Pooling Strategy for Patch Aggregation

Tab. 22 compares pooling strategies used to aggregate node-level features within each patch. The proposed weighted pooling consistently outperforms mean/max/min pooling, yielding the highest average score and zero performance drop. This confirms that learned, instruction-conditioned weighting is critical for preserving structurally salient signals, whereas uniform or extreme-value pooling discards fine-grained geometric cues required for accurate reasoning.

E.4. Maximum Patch Count

Tab. 23 evaluates the effect of the maximum allowable patch count. Performance is stable between 2048 and 4096 patches, indicating that Scaling-Aware Patching can effectively utilize additional capacity when available. However, reducing the budget below 1024 patches causes sharp degradation, particularly for proteins and nucleic acids, where structural complexity is higher. This demonstrates a clear trade-off between efficiency and representational sufficiency, and validates the default choice of 2048 as a balanced operating point for scaling-aware patching.

Table 25. Key limitations of Cuttlefish and corresponding future directions (three most reviewer-critical items).

Limitation	Why this is acceptable / common	Future work
No support for extremely large entities (e.g., > 50K nodes)	Scientific workflows and human interpretation typically focus on functional subregions (domains, active sites, loci) rather than a single-pass global readout; in our setting, LLM context and compute budgets further motivate segment-level reasoning.	Retrieval-augmented hierarchical reasoning (coarse-to-fine chunking, region proposals, iterative zoom-in) with memory-based summarization across passes.
Sensitivity to structure correctness / pre-processing choices	Structure-grounded modeling intrinsically depends on geometric fidelity; we therefore prioritize high-quality inputs (validated coordinates; controlled conformers) to avoid conflating model limitations with upstream structural noise.	Uncertainty-aware tokens (confidence/quality conditioning), multi-conformer / ensemble supervision, and structure-quality estimation are integrated into training and inference.
Reasoning supervision is coarse (no native all-atom reasoning corpus)	Large-scale, structure-grounded reasoning traces are scarce; our supervision is primarily format-stable and regularizes outputs, while most reasoning capacity is inherited from the backbone LLM.	Construct domain-grounded reasoning datasets and enforce evidence-based rationale learning with verifiable geometric attribution.

E.5. Effect of Training Stages

Table 24. Ablation on three training stages, evaluated on GEO-AT.

Training Stage	Molecule	Protein	DNA&RNA	Average	Avg. Drop
Cuttlefish	0.875	0.896	0.816	0.862	0
w/o LLM Adaptation	0.854	0.889	0.817	0.853	0.88%
w/o Alignment Tuning	0.742	0.787	0.801	0.777	8.54%
Random Encoder	0.376	0.382	0.565	0.441	42.11%

critical. LLM adaptation provides a smaller gain, suggesting it mainly refines instruction following after structural grounding is established.

Tab. 24 indicates that performance is dominated by structure-side representation learning and alignment. Replacing the pretrained encoder with a random encoder collapses the performance, confirming the necessity of modality pretraining. Removing alignment tuning yields a large drop as well, showing that initialized alignment is

F. Limitation and Future Work

F.1. Limitations

Cuttlefish integrates (i) geometry-grounded cross-modal alignment and (ii) instruction-conditioned scaling-aware patching to expose all-atom structure to a frozen LLM under an adaptive token budget. Despite improved structural faithfulness, Cuttlefish remains limited by extremely large entities, upstream structure quality, and weak reasoning supervision (Tab. 25). Beyond the three core limitations retained in the table, we note two additional constraints that are currently out of scope: (a) we do not explicitly model DNA folding or higher-order genome organization (e.g., chromatin-scale 3D ensembles), since most available all-atom nucleic-acid benchmarks emphasize local, structure-conditioned tasks; and (b) residual non-structural LLM hallucinations (factual/interpretive) may still occur in open-ended generation, even when structural hallucination is reduced.

F.2. Future Work

Tab. 25 suggests three actionable extensions: (i) extreme-scale structure understanding via hierarchical segmentation, retrieval, and iterative multi-pass summarization; (ii) robustness to upstream structure noise through uncertainty-aware tokens and multi-conformer/ensemble training; and (iii) domain-grounded reasoning supervision by building all-atom reasoning corpora with evidence-tethered rationales. In addition, two orthogonal directions remain important for broadening scope and trustworthiness: folding-aware, multi-scale nucleic-acid modeling (secondary/tertiary constraints and long-range contacts) and post-hoc verification (structure-consistency checks, tool-assisted validation, and uncertainty calibration) to further reduce residual hallucinations in open-ended generation.

G. Reproducibility

We release the full codebase, Cuttlefish checkpoints, and the proposed dataset GEO-AT at <https://anonymous.4open.science/r/Cuttlefish-455E/>. For double-blind review, the dataset and model artifacts are hosted via anonymous links, which are referenced from within the repository. The repository includes comprehensive

documentation and scripts to reproduce training, evaluation, and inference, including environment setup, preprocessing, command-line entry points, and configuration files for all reported experiments. All hyperparameters and implementation details not fully enumerated (e.g., LoRA settings) in the paper are specified in the released code and configs.